Electronic Supplementary Material (ESI) for Organic Chemistry Frontiers.

Supporting Information

Table of contents

1. Materials and general methods

All reagents and solvents were purchased from commercial sources and used without further purification. Manipulations were performed under normal atmosphere unless special noted. Merck 60 F_{254} foils were used for thin layer chromatography, and Merck 60 (230-400 mesh) silica gel was used for flash chromatography. Nuclear magnetic resonance (NMR) spectra were recorded at ambient temperature using Bruker AVANCE III 400/500 and Agilent DD2 600 spectrometers, with working frequencies of 400/500/600 and 100/125/150 MHz for ^{1}H and ^{13}C, respectively. Chemical shifts are reported in ppm relative to the residual internal non deuterated solvent signals (D_2O: δ = 4.79 ppm, DMSO-d_6: δ = 2.50 ppm, CD_3CN: δ = 1.94 ppm). High-resolution mass spectra (HRMS) were recorded on a Fourier transform ion cyclotron resonance mass spectrometry (FT-ICR MS) and LTC-Orbitrap Discovery mass spectrometer. HPLC purifications were performed on an Agilent 1260 Infinity II with a semipreparative column Luna® Omega 5 µm Polar C18 100 Å. UV/vis spectra were recorded on a Jasco V-650 spectrometer. Potentiometric measures were carried out with CRISON 5028 pH electrode for microsamples with Ag/AgCl reference element. X-ray crystallographic data were collected on a Bruker D8 Venture diffractometer.

2. Synthetic Procedures and characterization.

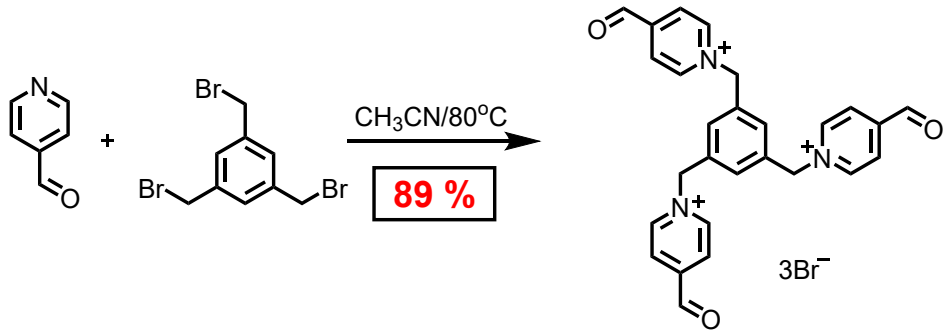

Scheme S1. Synthesis of $\mathbf{H_1}$·3Br.

$\mathbf{H_1}$·3Br: 4-pyridinecarboxaldehyde (1.50 g, 14 mmol) and 1,3,5-Tri(bromomethyl) benzene (500 mg, 1.4 mmol) were dissolved in 100 mL of acetonitrile and heated at reflux for 48 hours. The resulting precipitate was filtered and washed with hot acetonitrile (3 x 20 mL) to give the pure product $\mathbf{H_1}$·3Br (912 mg, 89 %) as a yellow powder. ^{1}H NMR (500 MHz, D_2O) δ (ppm): 8.84 (d, J = 5 Hz, 6H), 8.10 (d, J = 5 Hz, 6H), 7.54 (s, 3H), 6.15 (s, 3H), 5.81 (s, 6H). ^{13}C NMR (125 MHz, D_2O) δ (ppm): 160.60, 144.77, 135.36, 130.69, 125.72, 87.42, 63.05. HRMS (ESI): m/z calculated for $C_{27}H_{30}N_3O_6^{3+}$ $[M+3H_2O]^{3+}$ 164.0706, found 164.0707.

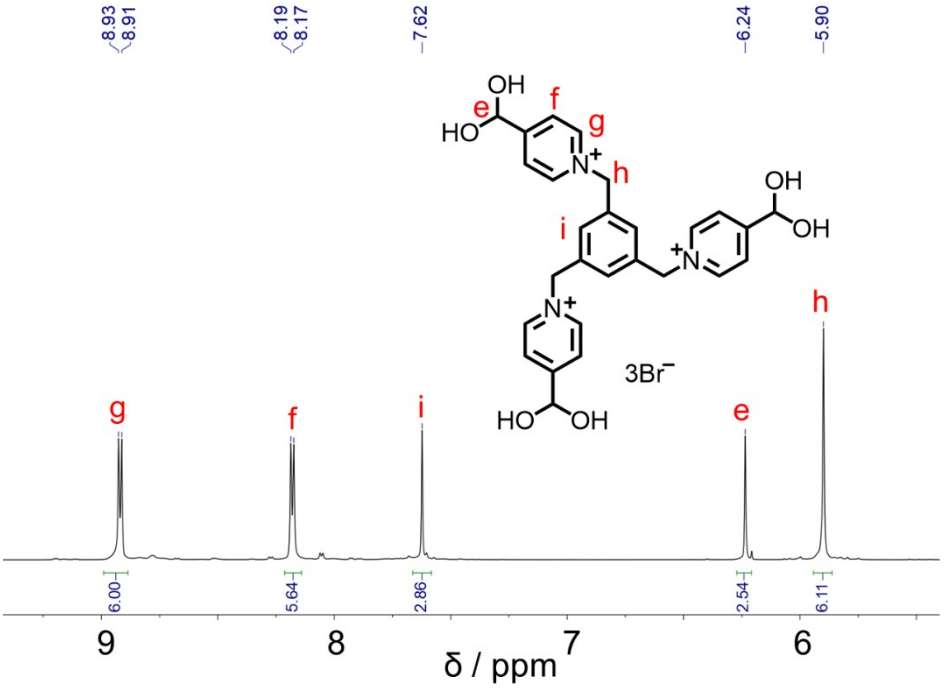

Figure S1. ^{1}H NMR (500 MHz, D_2O, 298 K) spectrum of $\mathbf{H_1}$·3Br.

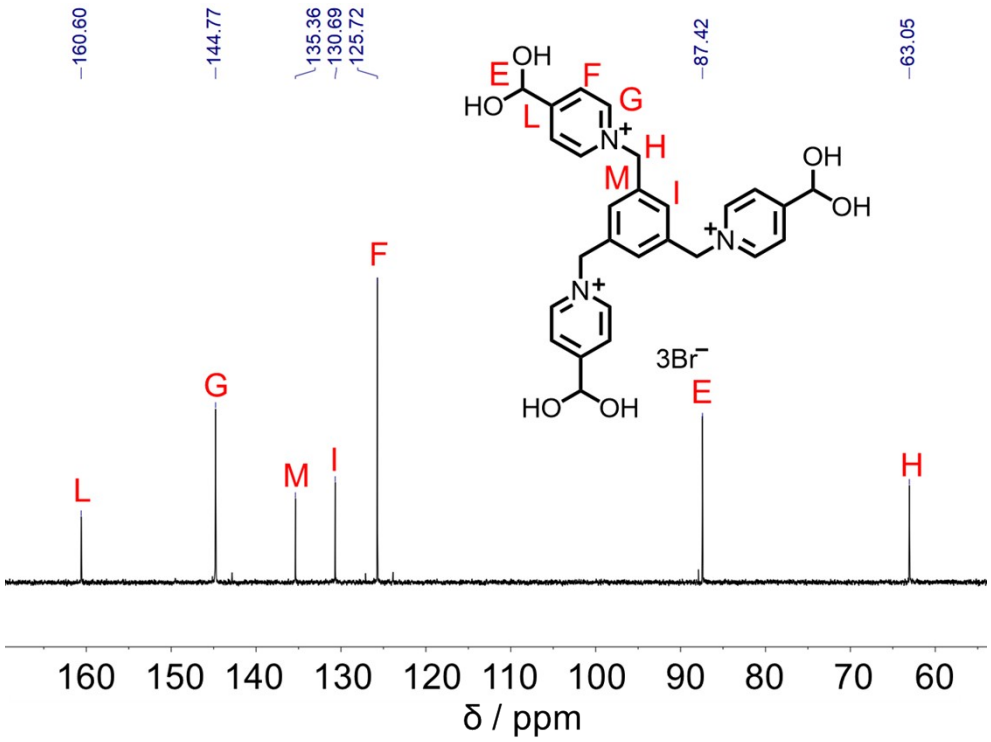

Figure S2. ^{13}C NMR (125 MHz, D_2O, 298 K) spectrum of **H_1**·3Br.

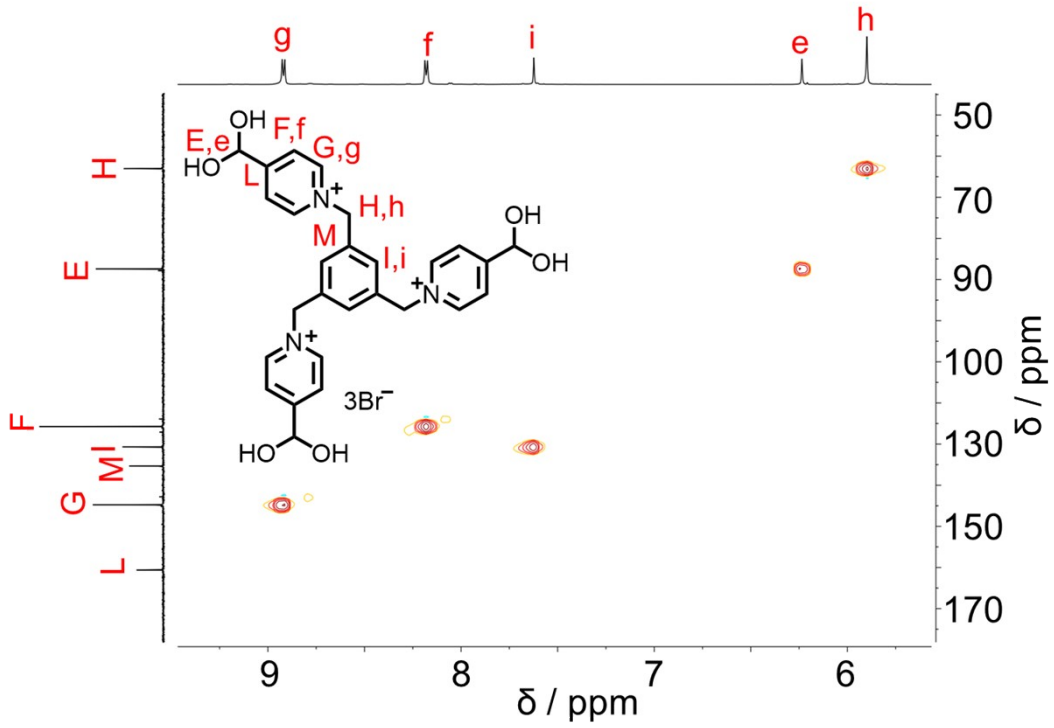

Figure S3. ^{1}H-^{13}C HSQC (500 and 125 MHz, D_2O, 298 K) spectrum of **H_1**·3Br.

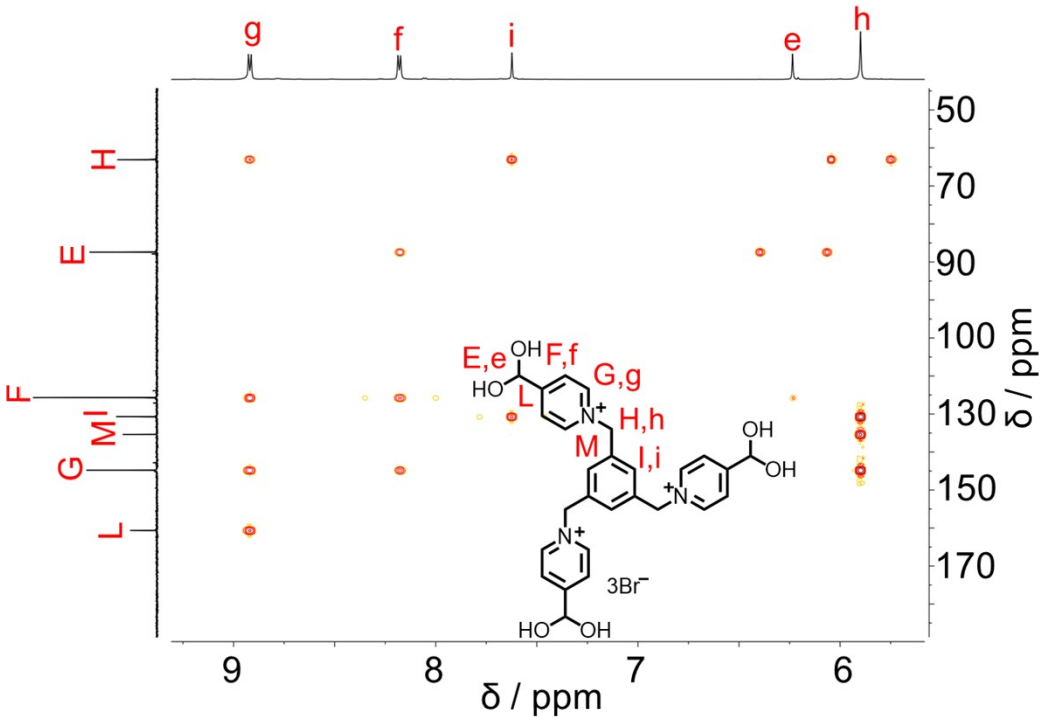

Figure S4. ^{1}H-^{13}C HMBC (500 and 125 MHz, D_2O, 298 K) spectrum of $\mathbf{H_1}$·3Br.

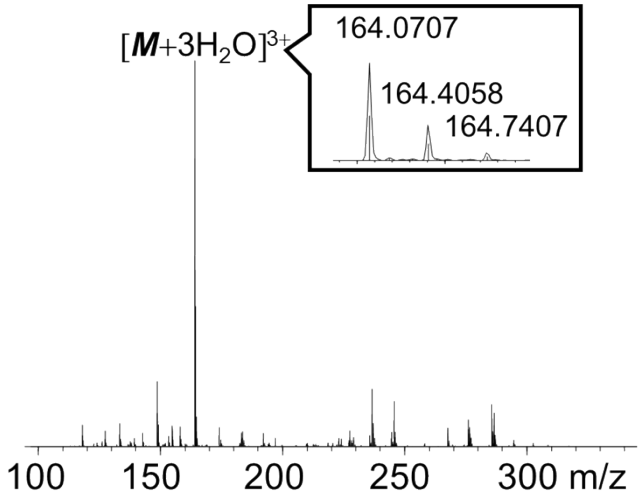

Figure S5. ESI-HRMS of $\mathbf{H_1}$·3Br.

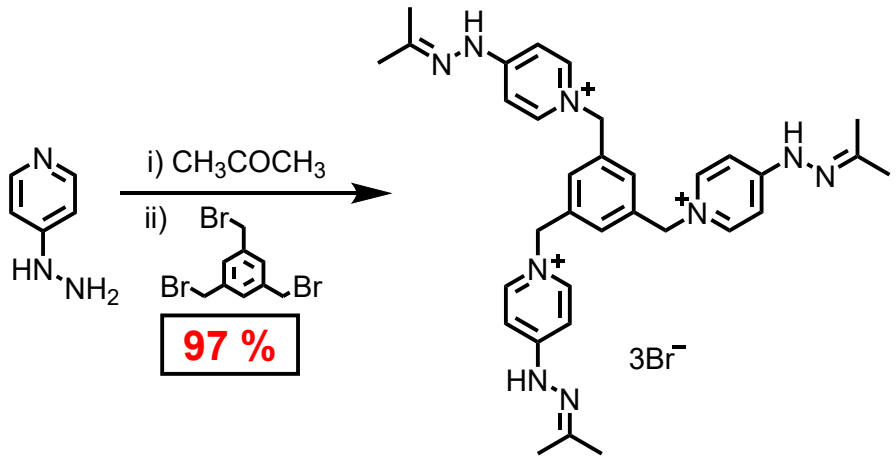

Scheme S2. Synthesis of **H_2**·3Br

H_2·3Br: A solution of 4-hydrazinopyridine (1.53g, 14.0 mmol) in 250 mL of acetone was heated at reflux for 1h. After this, 1,3,5-Tri(bromomethyl)benzene (500 mg, 1.4 mmol) was added to the reaction mixture and heated at reflux for 3 days. The obtained precipitate was filtrated upon cooling and washed with hot acetone (3 × 20 mL). The solvent was removed under reduce pressure to yielding virtually pure **H_2**·3Br (1.09 g, 97 %) as a yellow powder. ^{1}H NMR (500 MHz, DMSO) δ (ppm): 11.09 (s, 3H), 8.47(dd, J = 25 Hz, J = 5 Hz, 6H), 7.43(s, 3H), 7.40(dd, J = 25 Hz, J =5 Hz, 6H), 5.46(s, 6H), 2.06(d, J = 5 Hz, 18H). ^{13}C NMR (125 MHz, DMSO) δ (ppm): 167.59, 154.24, 143.98, 142.68, 137.13, 127.89, 108.99, 106.91, 59.20, 25.20, 18.22. **HRMS (ESI)**: *m/z* calculated for $C_{33}H_{42}N_9^{3+}$ $[M]^{3+}$ 188.1182, found 188.1155; calculated for $C_{33}H_{41}N_9^{2+}$ $[M–H]^{2+}$ 281.6737, found 281.6727; calculated for $C_{33}H_{40}N_9^{+}$ $[M–2H]^{+}$ 562.3401, found 562.3419.

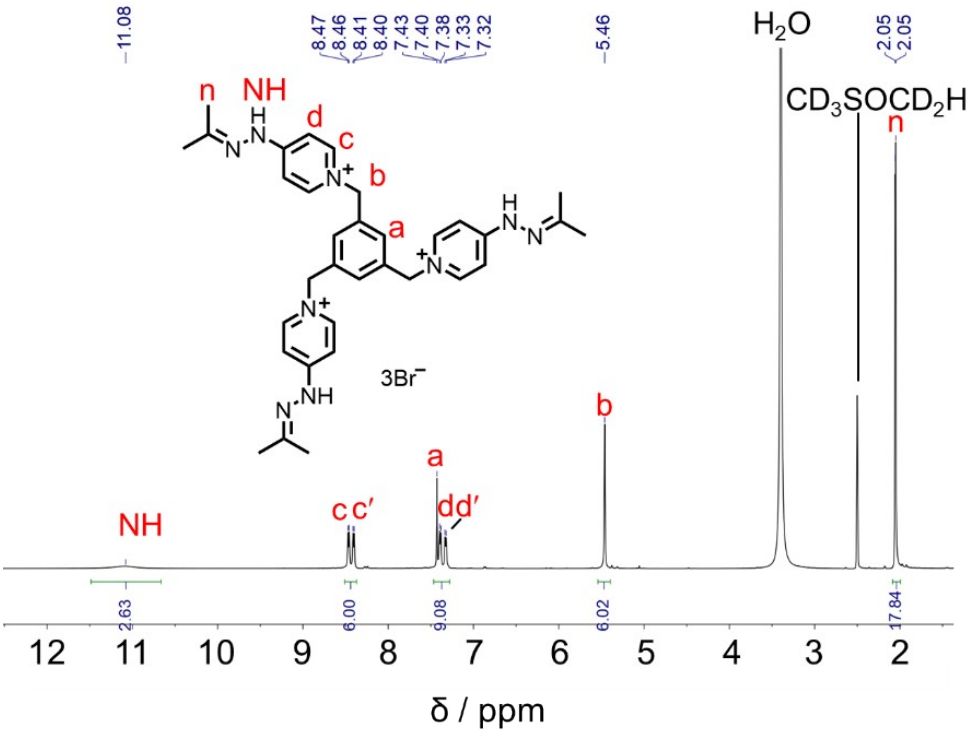

Figure S6. ^{1}H NMR (500 MHz, DMSO, 298 K) spectrum of **H_2**·3Br.

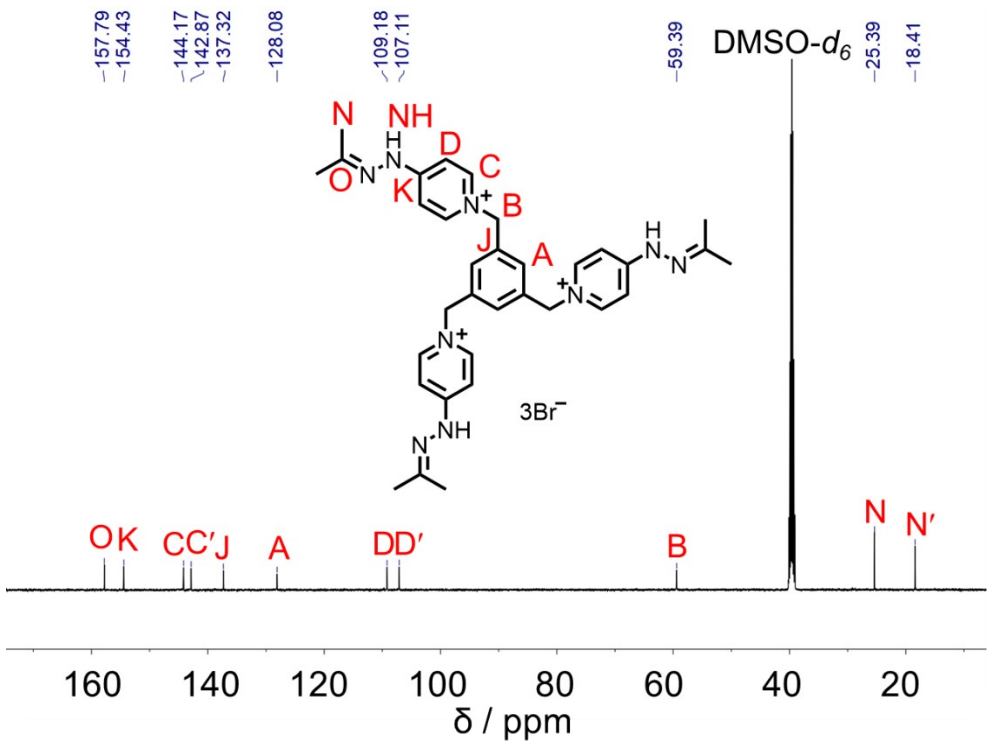

Figure S7. ^{13}C NMR (125 MHz, DMSO, 298 K) spectrum of **H_2**·3Br.

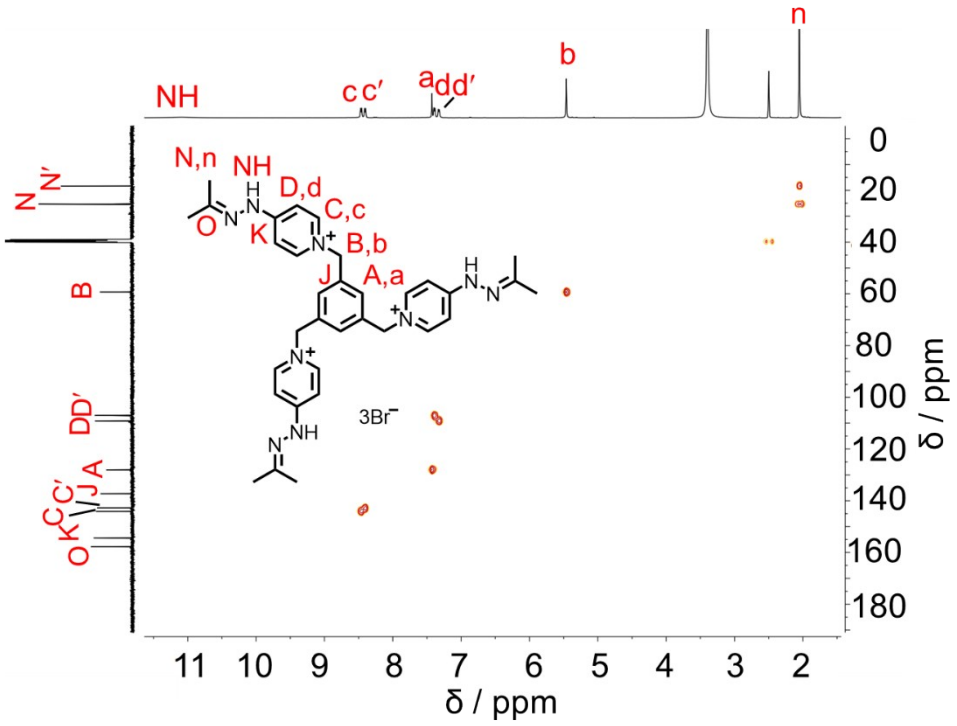

Figure S8. ^{1}H-^{13}C HSQC (500 and 125 MHz, DMSO, 298 K) spectrum of $\mathbf{H_2}$·3Br.

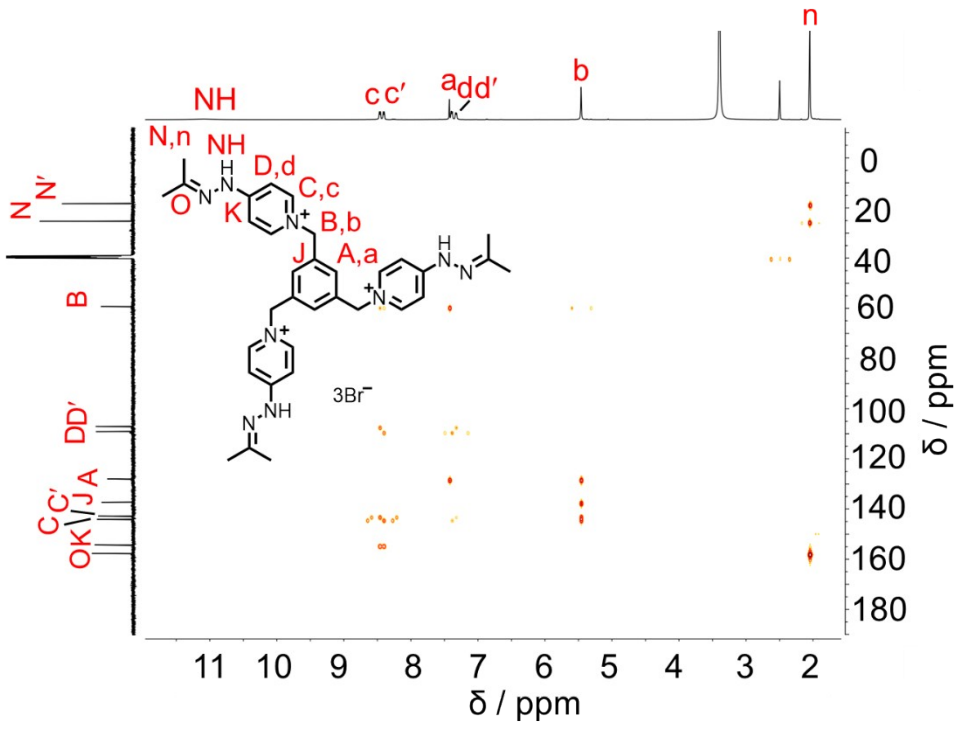

Figure S9. ^{1}H-^{13}C HMBC (500 and 125 MHz, DMSO, 298 K) spectrum of $\mathbf{H_2}$·3Br.

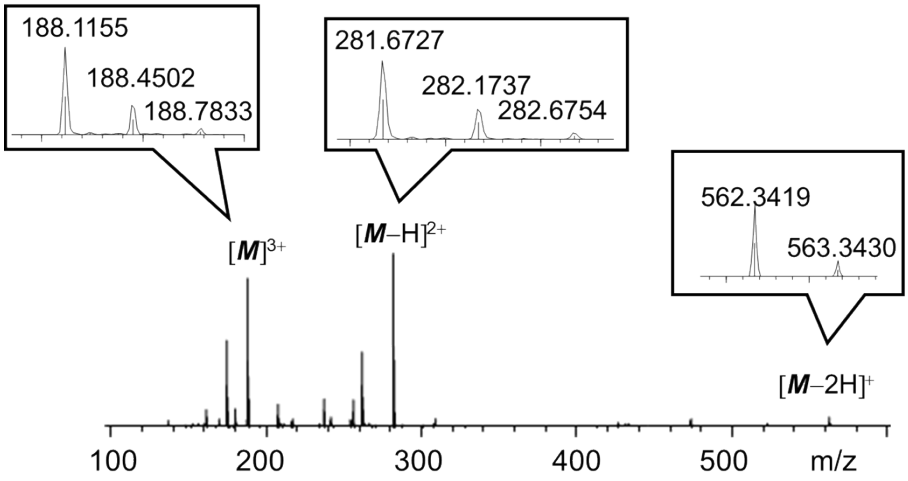

Figure S10. ESI-HRMS of $\mathbf{H_2}$·3Br.

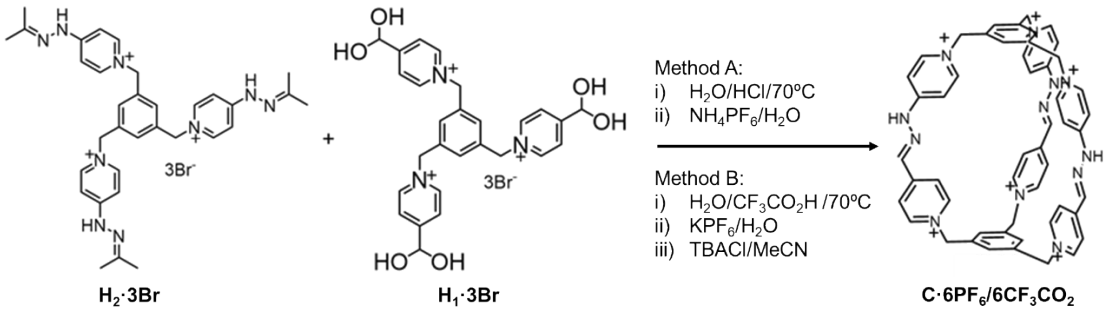

Scheme S3. Synthesis of $\mathbf{C}^{6+}$.

Method A:

C·6PF_6: A solution of **H_1**·3Br (82 mg, 0.12 mmol), **H_2**·3Br (100 mg, 0.12 mmol) and 1 mL of concentrated HCl in 50 mL of water was heated at 70 ºC for 12 h. After cooling, excess of NH_4PF_6 was added until no further precipitation was observed. The obtained solid was filtrated and washed with water (3 × 10 mL). The crude sample was purified by flash column chromatography (H_2O/methanol/nitromethane (12:7:1); 200-300 mesh), followed by counteranoin exchange, yielding the pure **C**·6PF_6 (110 mg, 52%) as a reddish solid.

^{1}H NMR (500 MHz, CD_3CN) δ (ppm) 8.44 (d, J = 5.5 Hz, 3H), 8.40 (d, J = 7.0 Hz, 6H), 8.31 (d, J = 7.0 Hz, 6H), 8.22 (s, 3H), 7.93 (d, J = 5.5 Hz, 3H), 7.80 (s, 3H), 7.68 (s, 3H), 7.56 (d, J = 6.5 Hz, 3H), 7.27 (d, J = 7.5 Hz, 3H), 5.69 (s, 6H), 5.44 (s, 6H). ^{13}C NMR (100 MHz, CD_3CN) δ (ppm): 156.16, 151.23, 145.57, 145.03, 143.29, 140.85, 136.47, 135.82, 135.78, 134.91, 125.91, 111.56, 111.36, 63.59, 61.56. HRMS (ESI): *m/z* calculated for $C_{51}H_{47}F_6N_{12}P^{4+}$ [*M*-H+PF_6]$^{4+}$ 243.0917, found 243.0881; $C_{51}H_{46}F_6N_{12}P^{3+}$ [*M*-2H+PF_6]$^{3+}$ 323.1786, found 323.7861; $C_{51}H_{48}F_{18}N_{12}P_3^{3+}$ [*M*+3PF_6]$^{3+}$ 421.1011, found 421.1026; $C_{51}H_{45}F_6N_{12}P^{3+}$ [*M*-3H+PF_6]$^{3+}$ 485.1760, found 485.1722.

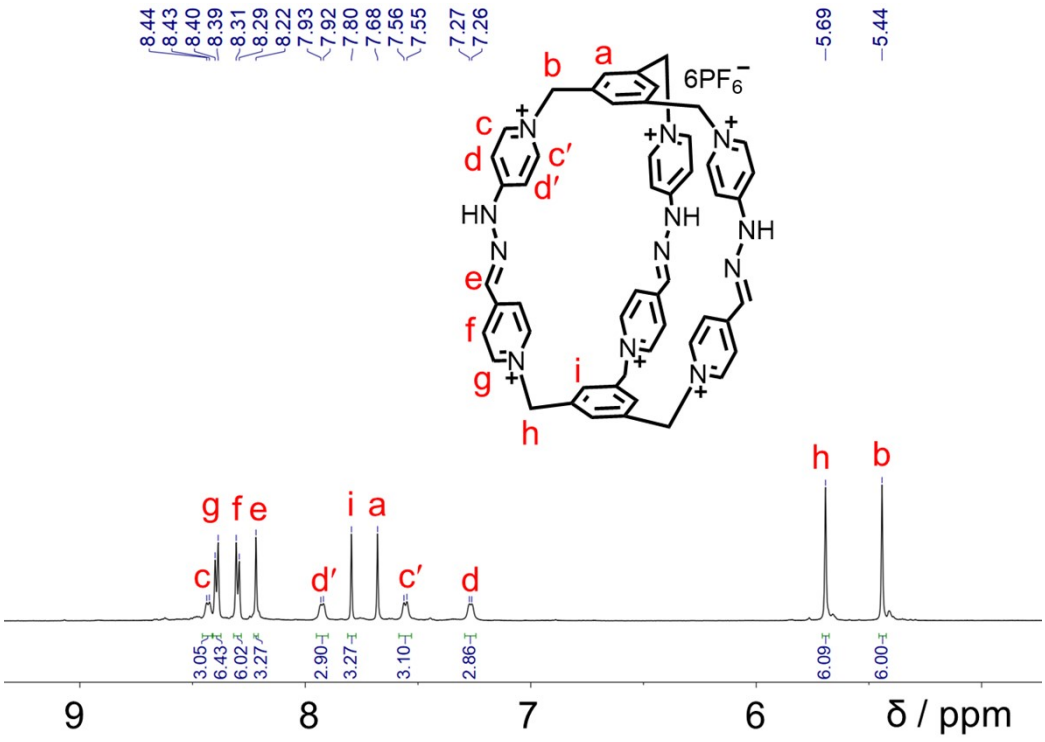

Figure S11. ^{1}H NMR (500 MHz, CD_3CN, 298 K) spectrum of **C**·6PF_6.

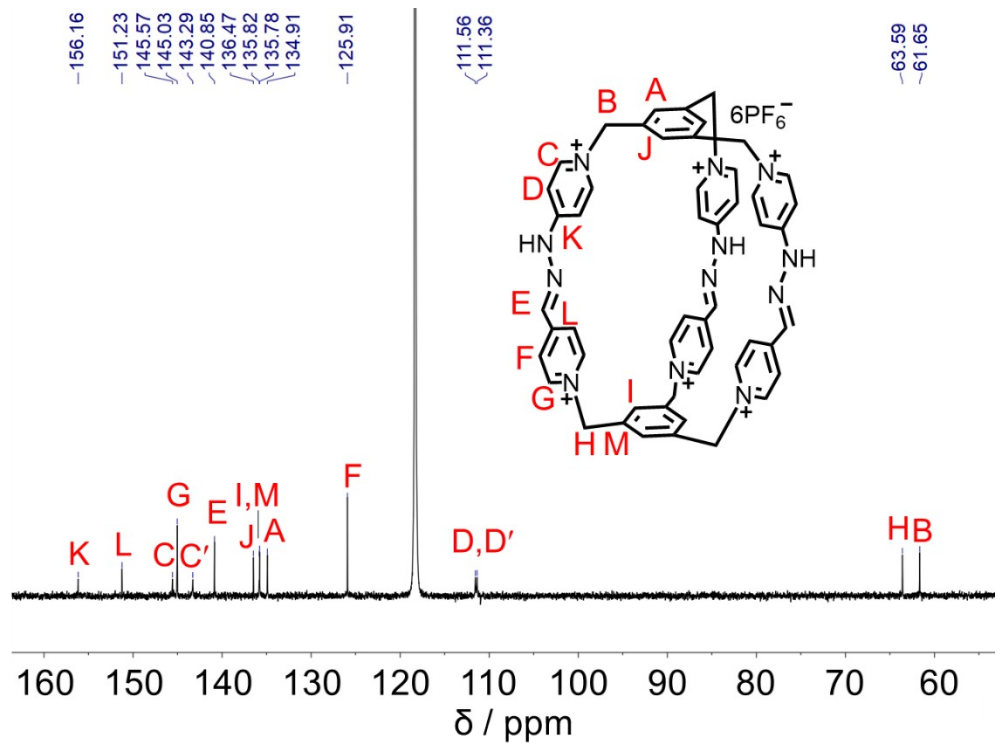

Figure S12. ^{13}C NMR (500 MHz, CD_3CN, 298 K) spectrum of **C**·6PF_6.

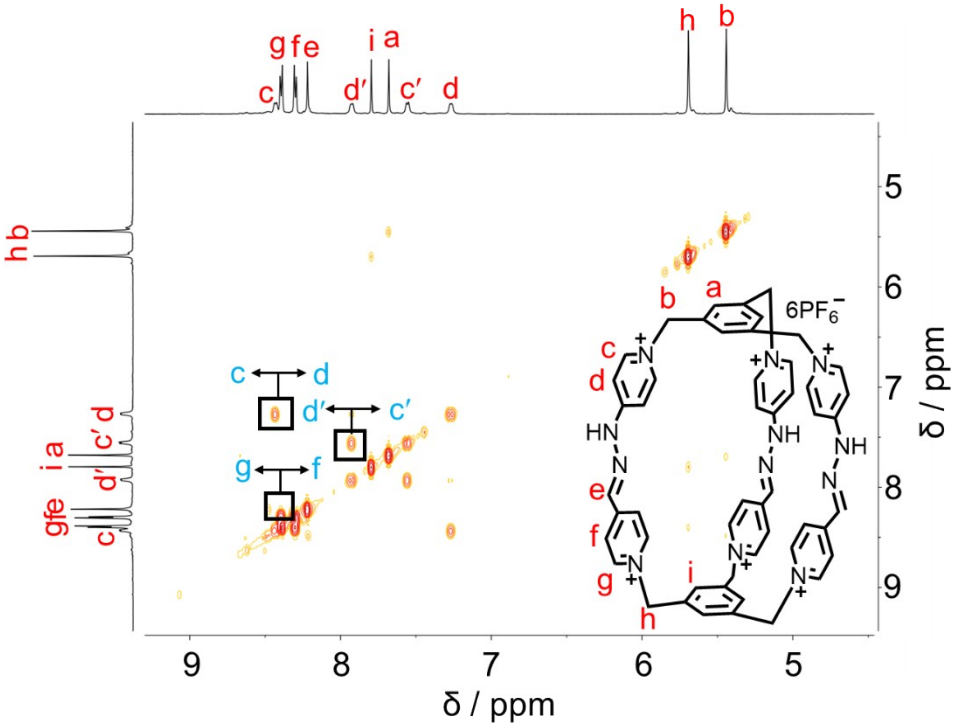

Figure S13. ^{1}H-^{1}H COSY (500 MHz, CD_3CN, 298 K) spectrum of **C**·6PF_6. Key correlation peak is labeled in the spectrum.

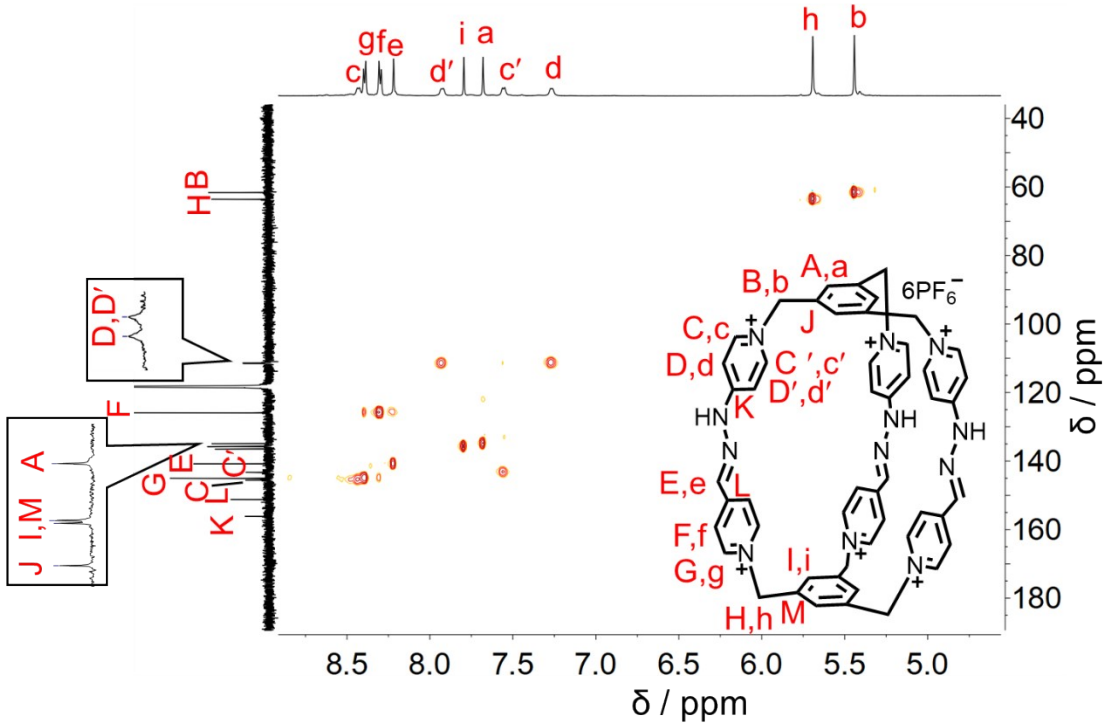

Figure S14. ^{1}H-^{13}C HSQC (500 and 125 MHz, DMSO, 298 K) spectrum of **C**·6PF_6.

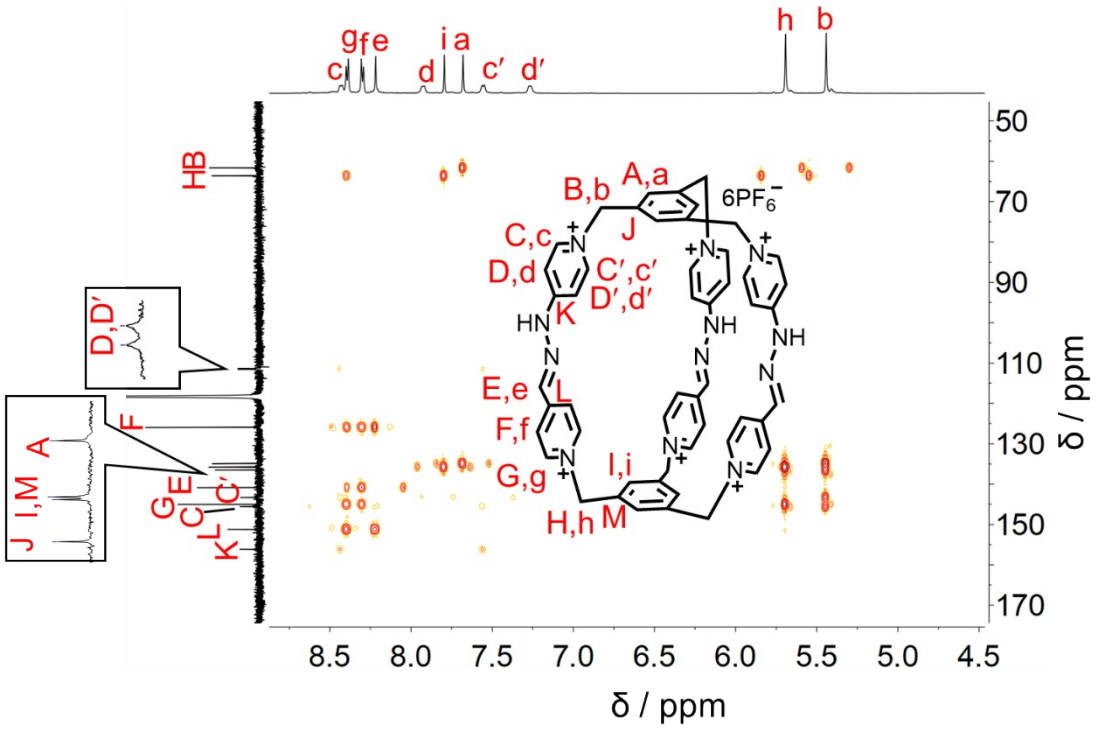

Figure S15. ^{1}H-^{13}C HMBC (500 and 125 MHz, DMSO, 298 K) spectrum of **C**·6PF_6.

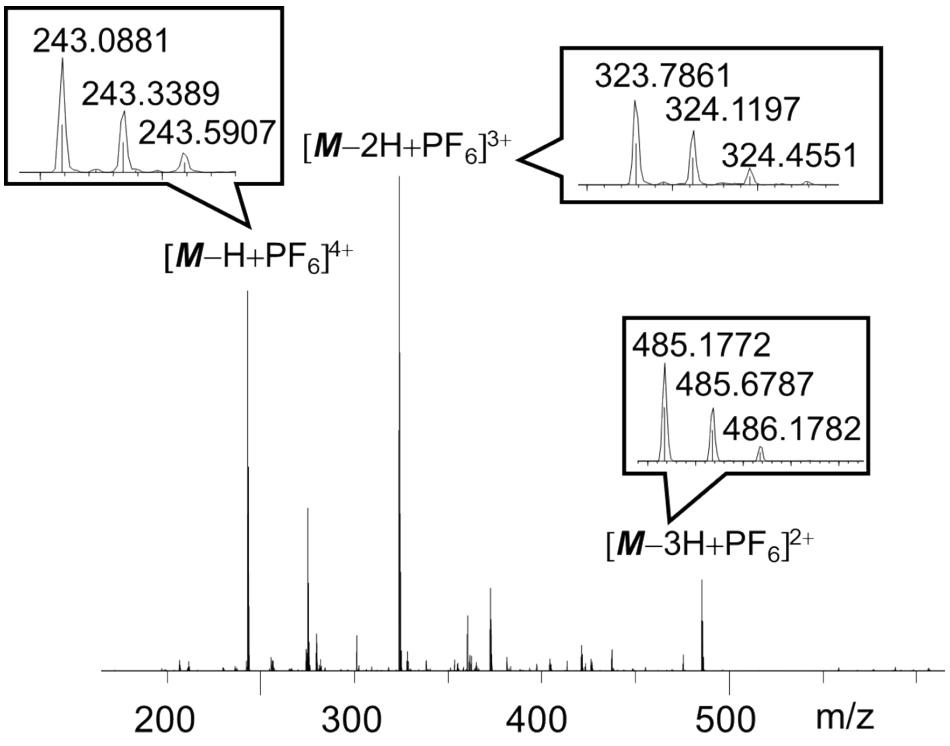

Figure S16. ESI-HRMS of **C**·6PF_6.

C·6Cl could be obtained via counteranion exchange, which was accomplished by adding either TBACl into the solution of **C**·6PF_6 in acetonitrile, followed by filtration to collect the corresponding precipitates. ^{1}H NMR (500 MHz, D_2O, 298K) δ (ppm) 8.67 (d, J = 5 Hz, 6H), 8.61 (s, 3H), 8.26 (d, J = 5 Hz, 6H), 8.24 (s, 3H), 7.91 (s, 3H), 7.77 (s, 6H), 7.75 (s, 3H), 7.22 (s, 3H), 5.86 (s, 6H), 5.55 (s, 6H). HRMS (ESI): *m/z* calculated for $C_{51}H_{46}N_{12}^{4+}$ [*M*-2H]$^{4+}$ 206.5987, found 206.5965; $C_{51}H_{45}N_{12}^{3+}$ [*M*-3H]$^{3+}$ 275.1291, found 275.1261.

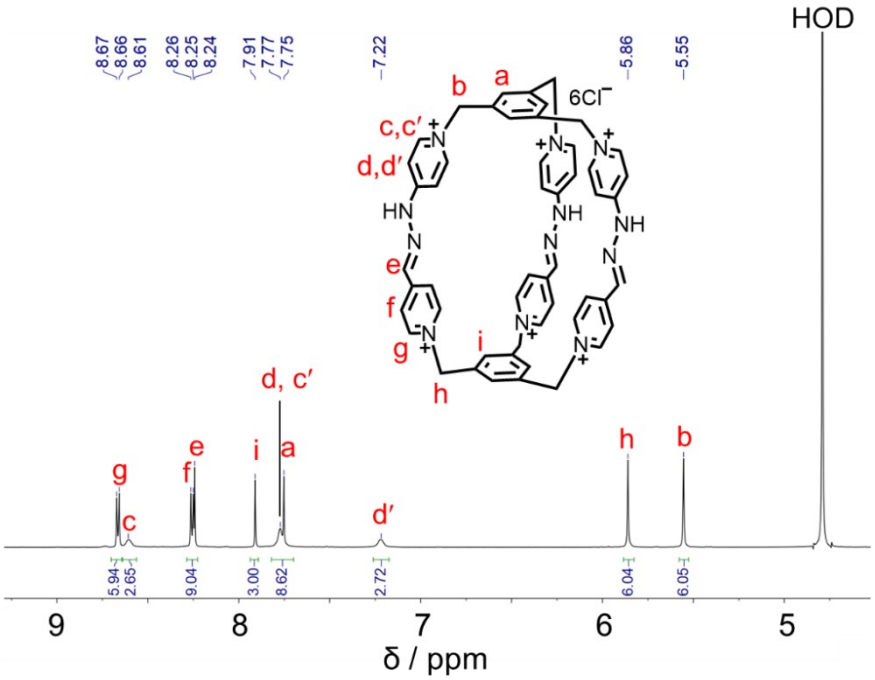

Figure S17. ^{1}H NMR (500 MHz, D_2O, 298 K) spectrum of **C**·6Cl

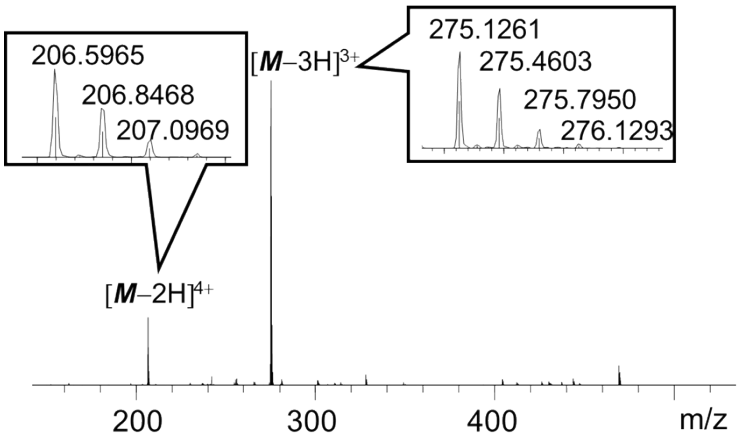

Figure S18. ESI-HRMS of **C**·6Cl.

Method B:

H_1·3Br (376 mg, 0.51 mmol) and **H_2**·3Br (413 mg, 0.51 mmol) were dissolved in H_2O (180 mL, 2.8 mM). TFA (4 µL, 0.05 mmol) was added. The solution was stirred and heated at 70 ºC for 24 h. After cooling, excess of KPF_6 was added until no more precipitate was formed. The solid was filtered and washed with H_2O and Et_2O. The solid was redissolved in MeCN and an excess of TBACl was added until no more precipitate was formed. The solid was washed with MeCN and Et_2O.

A fraction of the solid (51.1 mg) was dissolved in H_2O:MeCN 2:1 and purified by reverse-phase semipreparative HPLC (A: H_2O + 0.1% TFA, B: MeCN + 0.1% TFA), giving a yellowish solid (35.5 mg, 48%, **C**·$6CF_3CO_2$).

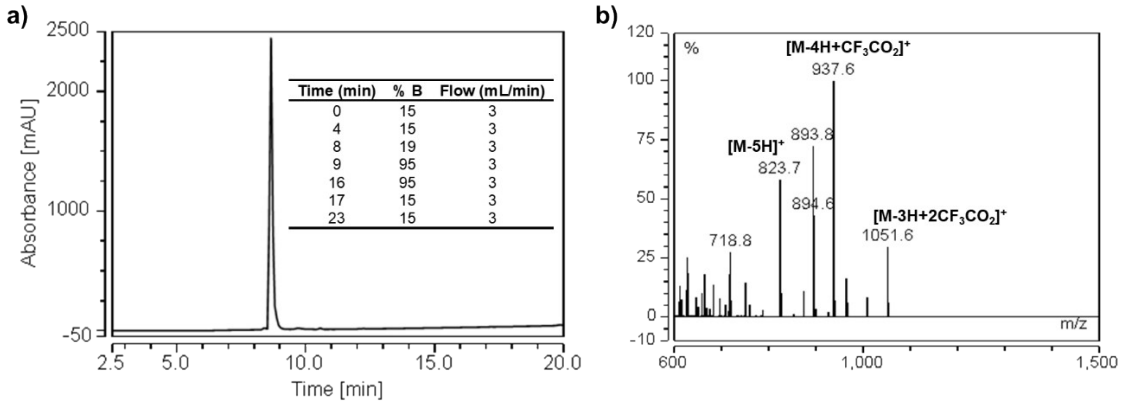

Figure S19. a) HPLC chromatogram (200 nm) of purified **C^{6+}** with t_r = 8.8 min. (Inset) Purification method. b) MS spectrum from the chromatographic peak at t_r = 8.8 min.

- **C**·$6CF_3CO_2$ characterization at pD = 2 (NaH_2PO_4/H_3PO_4 buffer) in D_2O by NMR and HRMS:

^{1}H NMR (500 MHz, D_2O) δ (ppm): 8.62 (d, *J* = 6.5 Hz, 6H), 8.56 (d, *J* = 7.1 Hz, 3H), 8.15 (s, 3H), 8.11 (d, *J* = 6.4 Hz, 6H), 7.79 (s, 3H), 7.74 (d, *J* = 7.3 Hz, 3H), 7.63 (s, 3H), 7.59 – 7.54 (m, 3H), 7.15 (d, *J* = 7.0 Hz, 3H), 5.77 (s, 6H), 5.47 (s, 6H). ^{13}C NMR (126 MHz, D_2O) δ (ppm): 154.48, 150.08, 144.11, 143.99, 142.54, 140.15, 136.48, 135.91, 132.49, 131.65, 110.20, 109.92, 62.89, 60.89. HRMS (ESI): *m/z* calculated for $C_{52}H_{45}F_3N_{12}O_2^{2+}$ [*M*-3H+CF_3O_2]$^{2+}$ 469.1865, found 469.1864; $C_{51}H_{45}N_{12}^{3+}$ [*M*-3H]$^{3+}$ 275.1291, found 275.1289; $C_{51}H_{44}N_{12}^{3+}$ [*M*-4H]$^{3+}$ 412.1900, found 412.1900

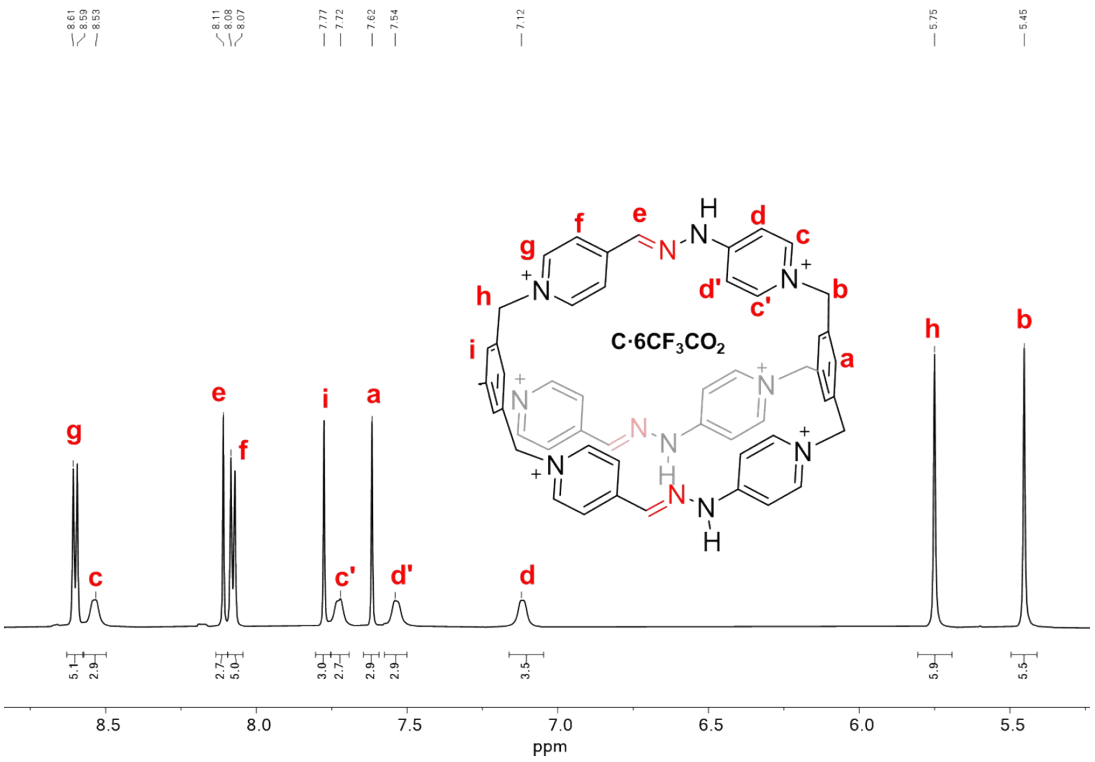

Figure S20. ^{1}H NMR (500 MHz, D_2O, 298 K) spectrum of **C**·6CF_3CO_2.

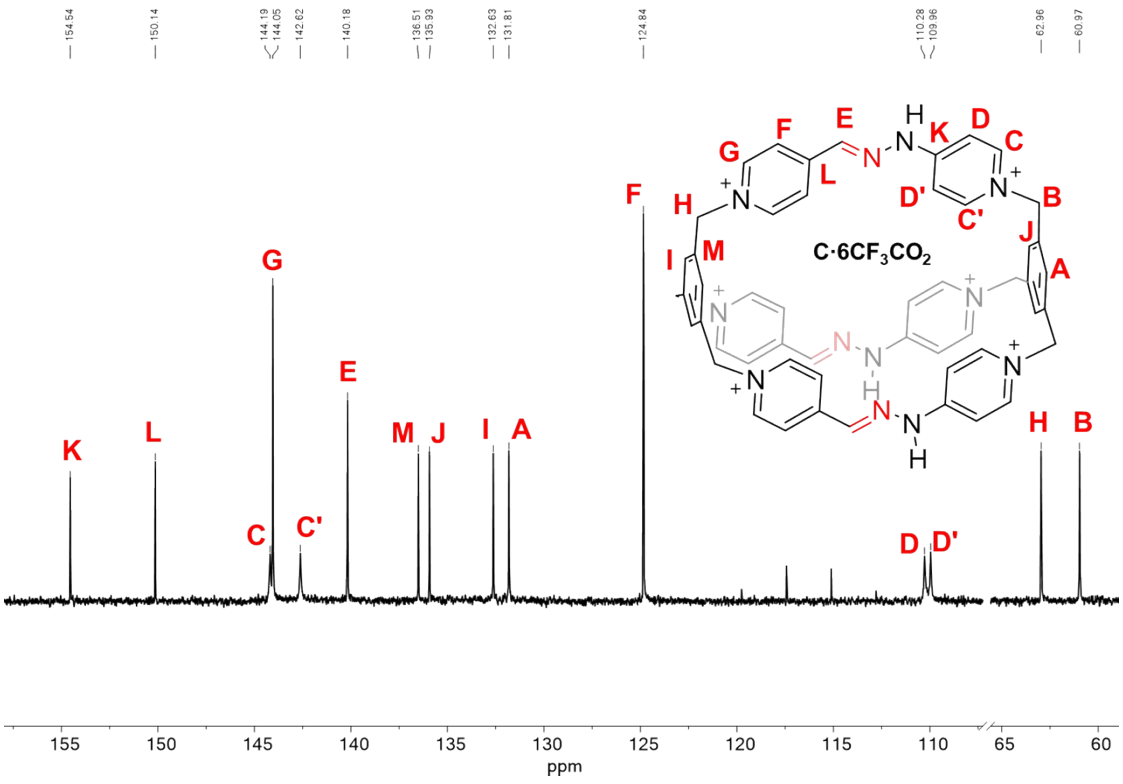

Figure S21. ^{13}C NMR (125 MHz, D_2O, 298 K) spectrum of **C**·6CF_3CO_2.

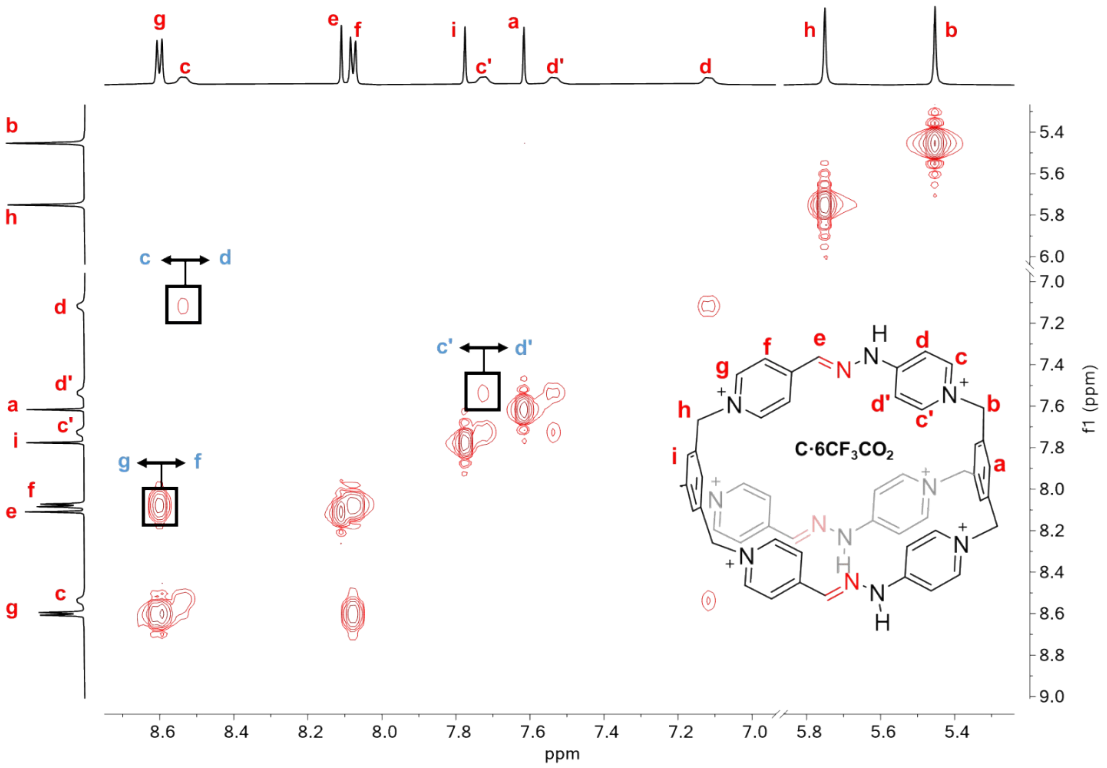

Figure S22. ^{1}H-^{1}H COSY (500 MHz, D_2O, 298 K) spectrum of **C**·6CF_3CO_2. Key correlation peak is labeled in the spectrum.

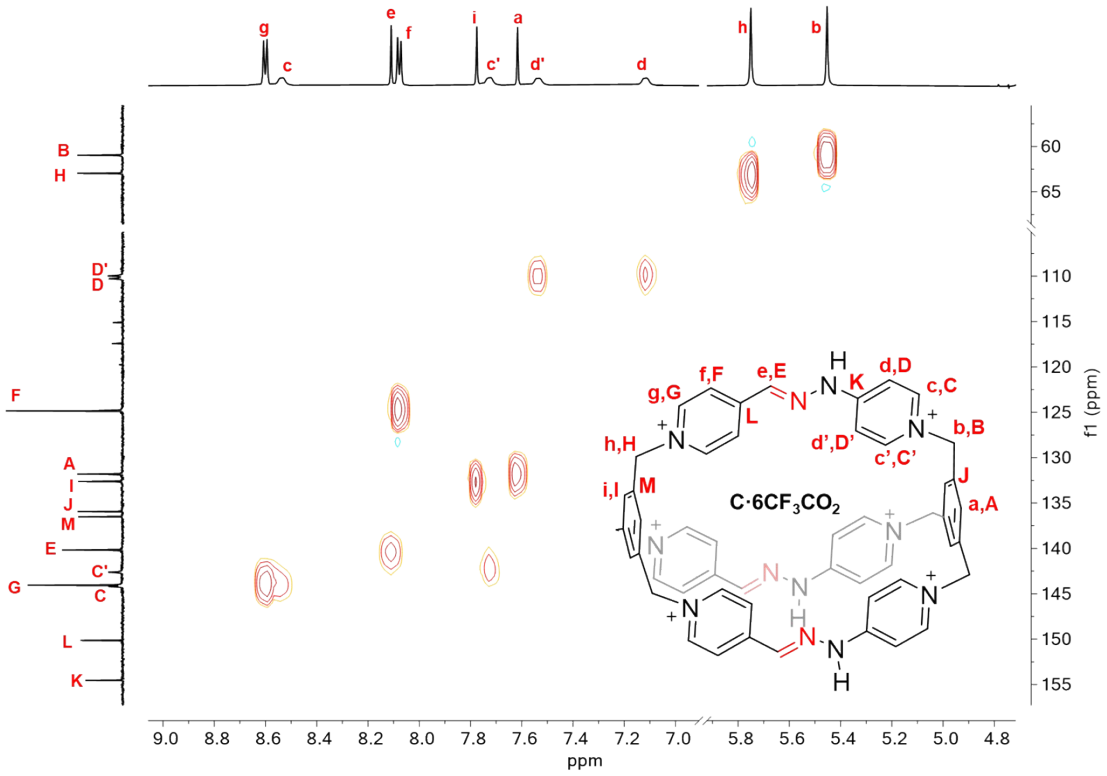

Figure S23. ^{1}H-^{13}C HSQC (500 and 125 MHz, D_2O, 298 K) spectrum of **C**·6CF_3CO_2.

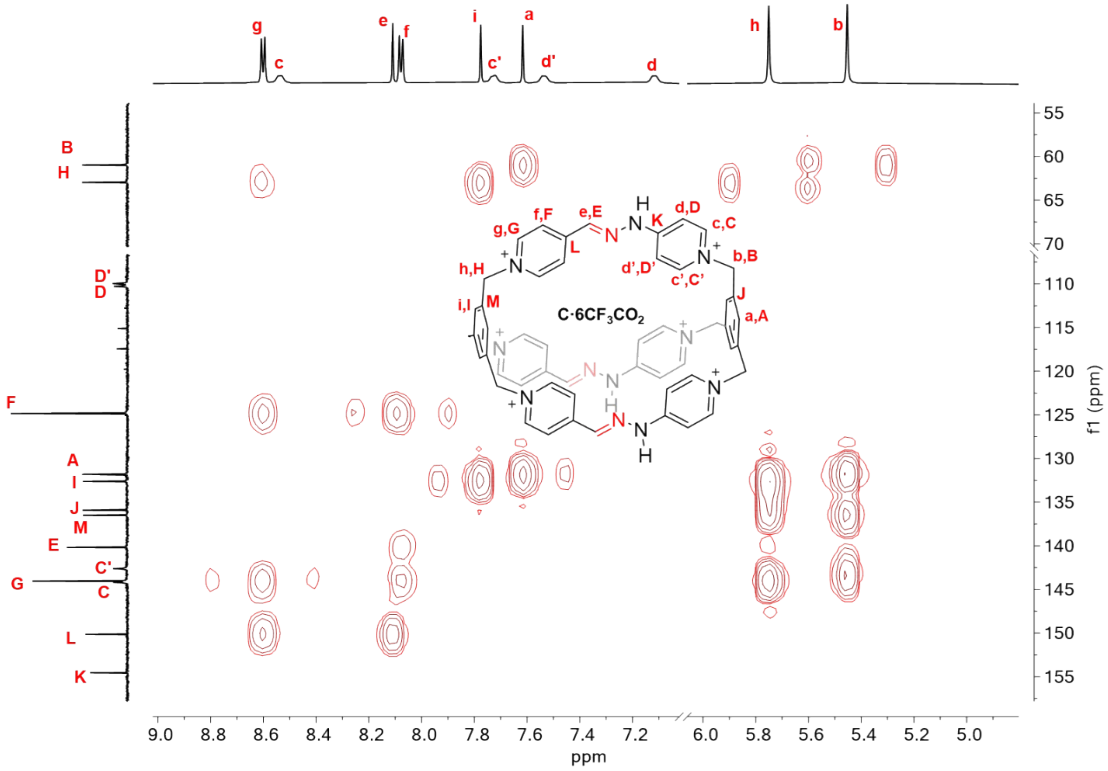

Figure S24. ^{1}H-^{13}C HMBC (500 and 125 MHz, D_2O, 298 K) spectrum of **C**·6CF_3CO_2.

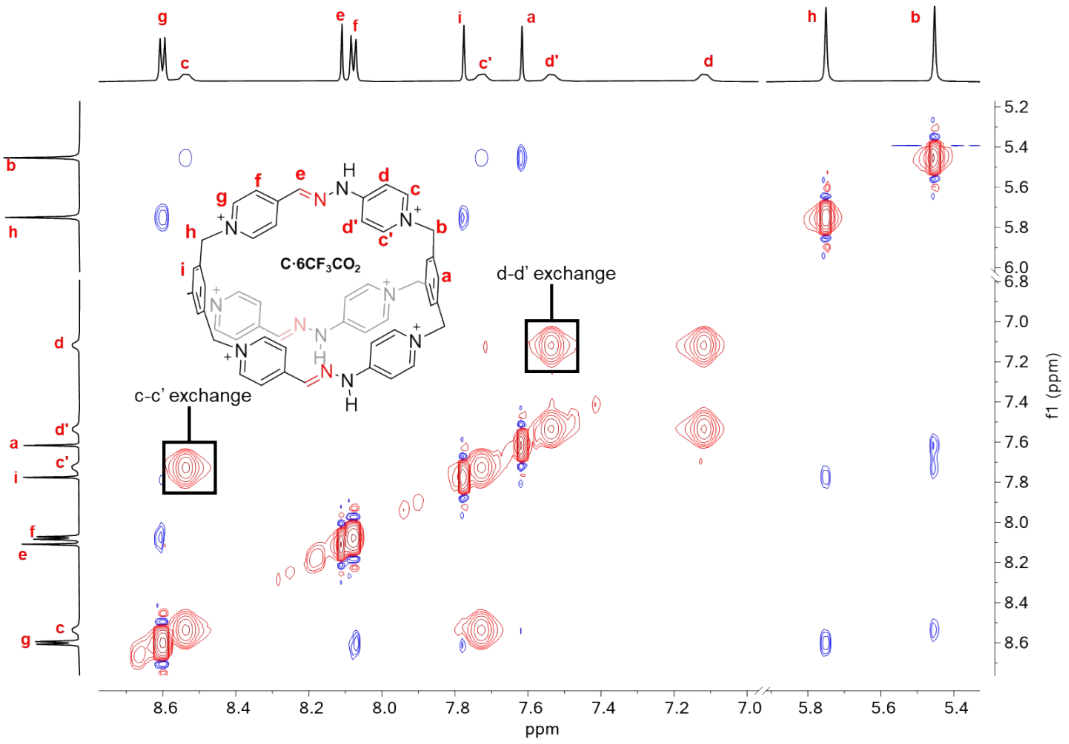

Figure S25. ^{1}H-^{1}H NOESY (500 MHz, D_2O, 298 K) spectrum of **C**·6CF_3CO_2. Exchange cross-peak is labeled in the spectrum.

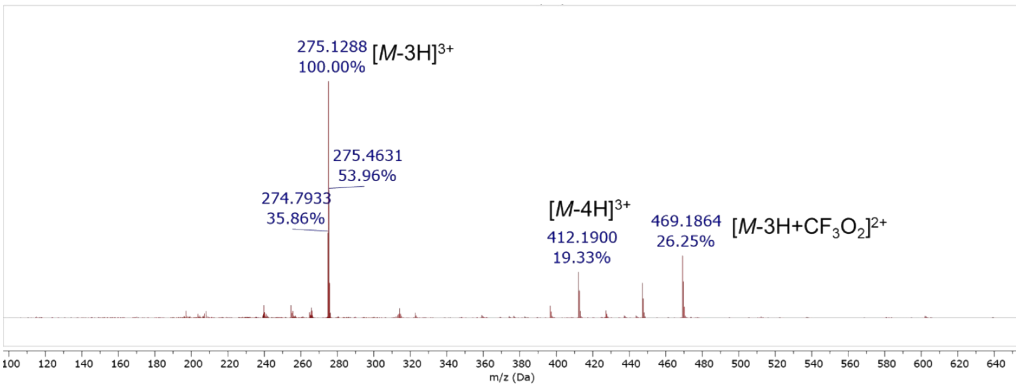

Figure S26. ESI-HRMS of **C**·6CF_3CO_2.

- **C**·3CF_3CO_2 characterization at pD = 12 (Na_3PO_4/Na_2HPO_4 buffer) in D_2O by NMR: ^{1}H NMR (500 MHz, D_2O) δ (ppm): 8.36 (d, J = 7.1 Hz, 1H), 8.03 (s, 1H), 8.00 (d, J = 7.2 Hz, 1H), 7.91 (d, J = 5.6 Hz, 1H), 7.64 (s, 1H), 7.43 (s, 1H), 7.22 (s, 1H), 7.17 (d, J = 7.6 Hz, 1H), 6.68 (d, J = 7.1 Hz, 1H), 5.61 (s, 1H), 5.13 (s, 1H). ^{13}C NMR (126 MHz, D_2O) δ (ppm): 164.34, 152.30, 142.75, 141.54, 139.99, 139.32, 137.78, 137.03, 130.84, 129.41, 122.93, 113.03, 109.25, 62.26, 59.58.

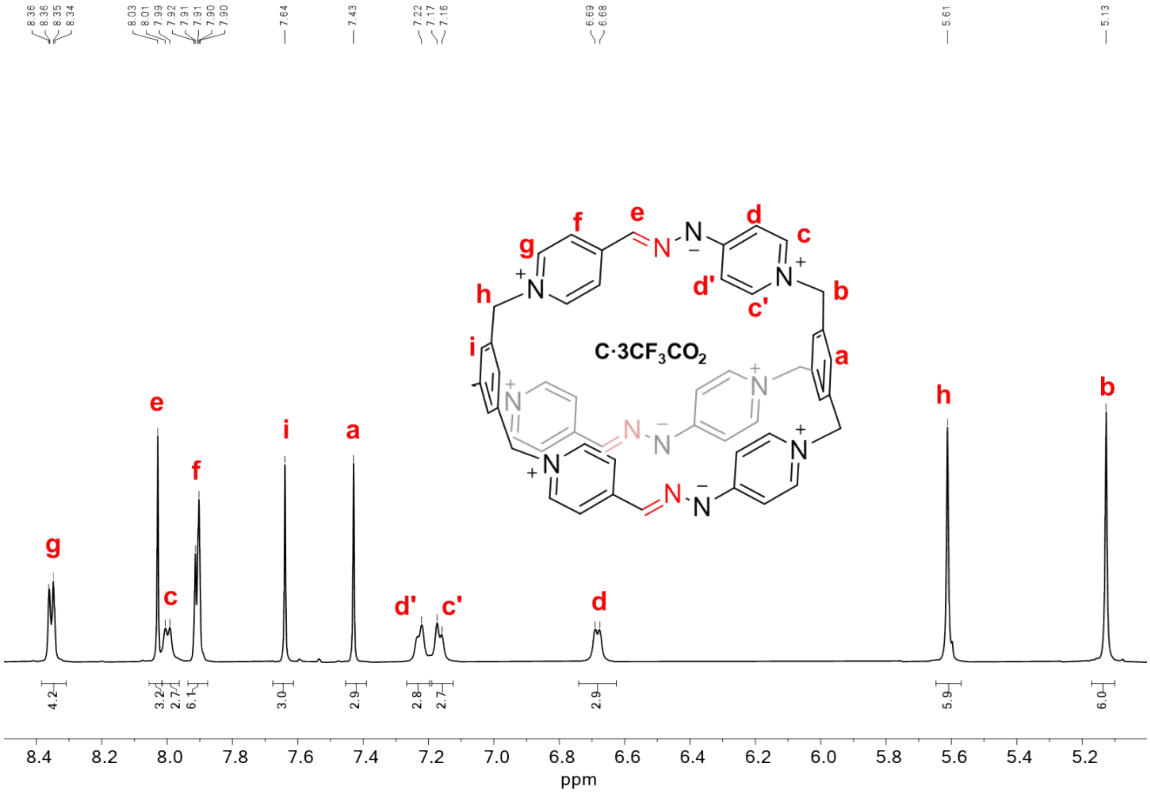

Figure S27. ^{1}H NMR (500 MHz, D_2O, 298 K) spectrum of **C**·3CF_3CO_2.

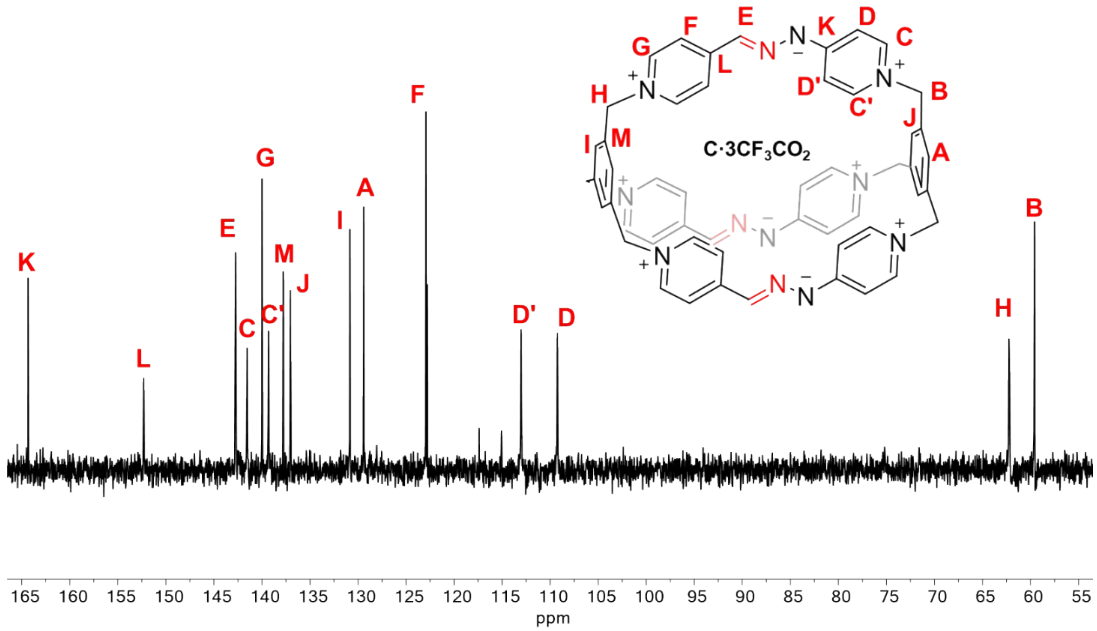

Figure S28. ^{13}C NMR (125 MHz, D_2O, 298 K) spectrum of **C**·$3CF_3CO_2$.

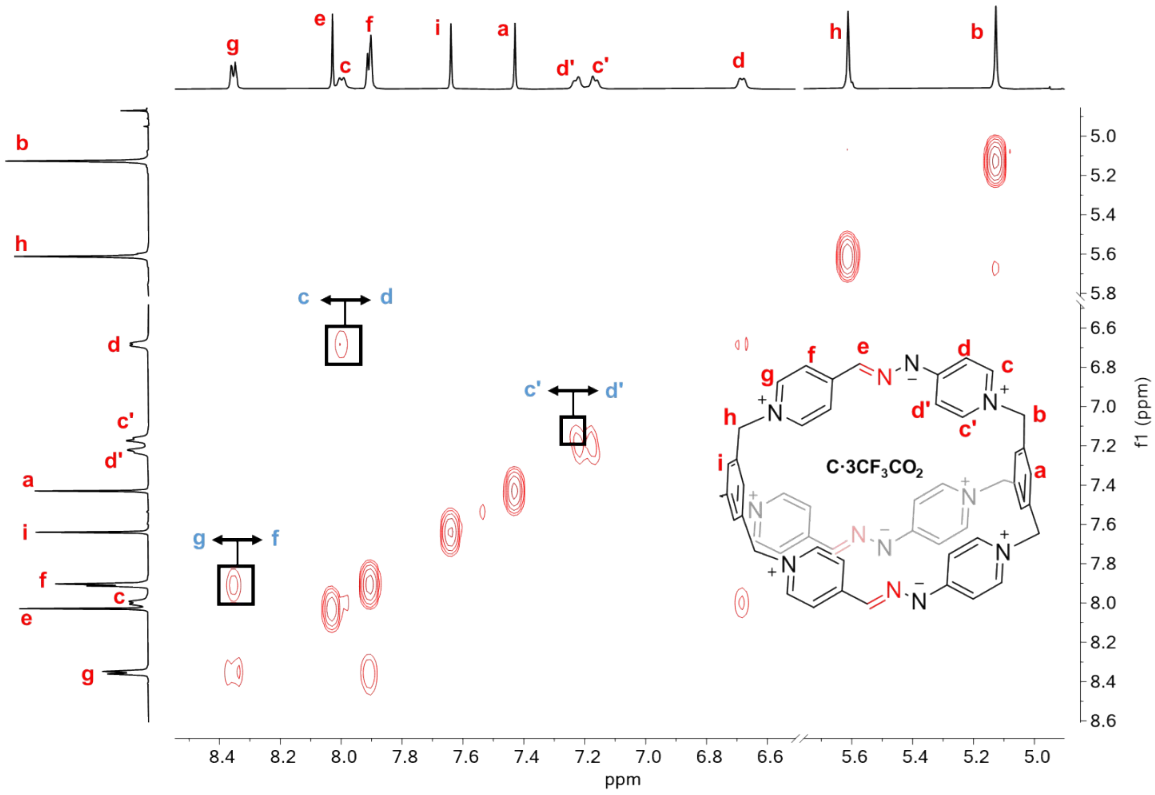

Figure S29. ^{1}H-^{1}H COSY (500 MHz, D_2O, 298 K) spectrum of **C**·$3CF_3CO_2$. Key correlation peak is labeled in the spectrum.

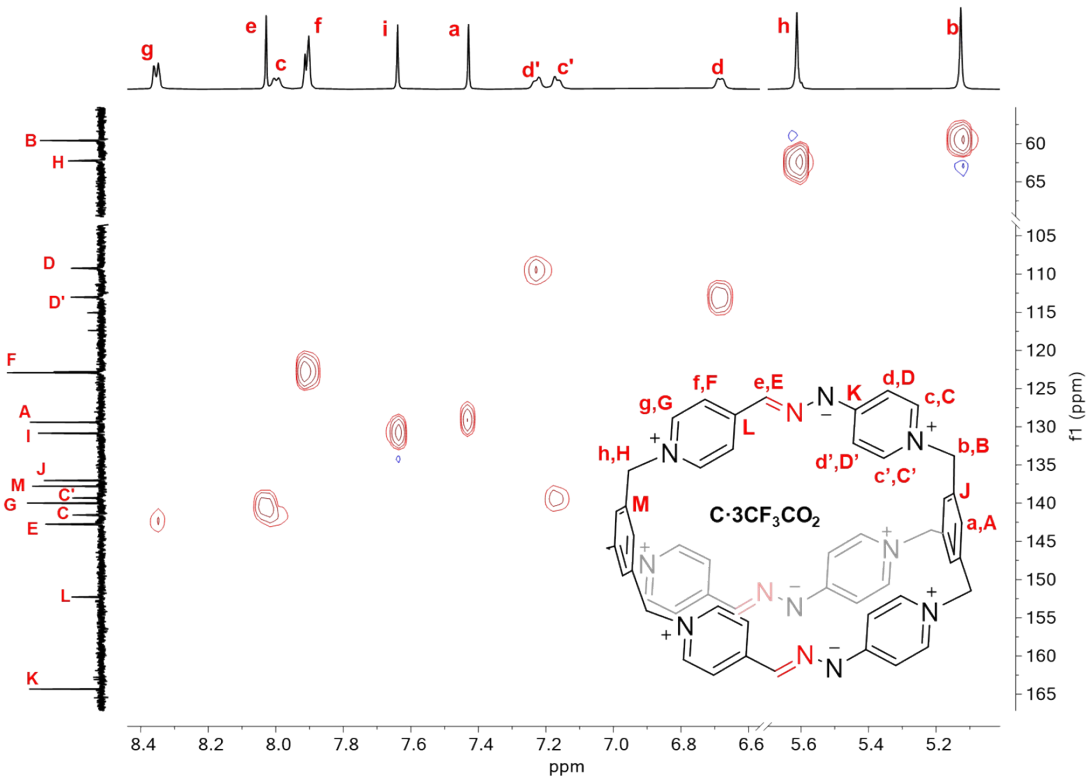

Figure S30. ^{1}H-^{13}C HSQC (500 and 125 MHz, D_2O, 298 K) spectrum of **C**·$3CF_3CO_2$.

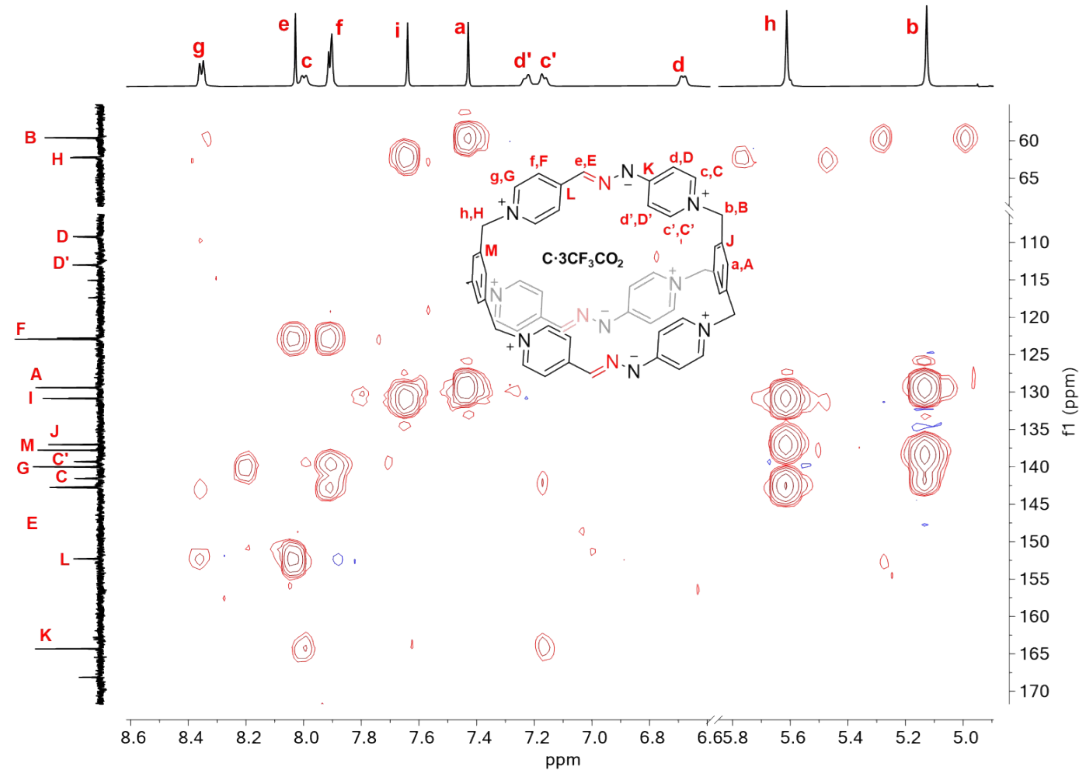

Figure S31. ^{1}H-^{13}C HMBC (500 and 125 MHz, D_2O, 298 K) spectrum of **C**·$3CF_3CO_2$.

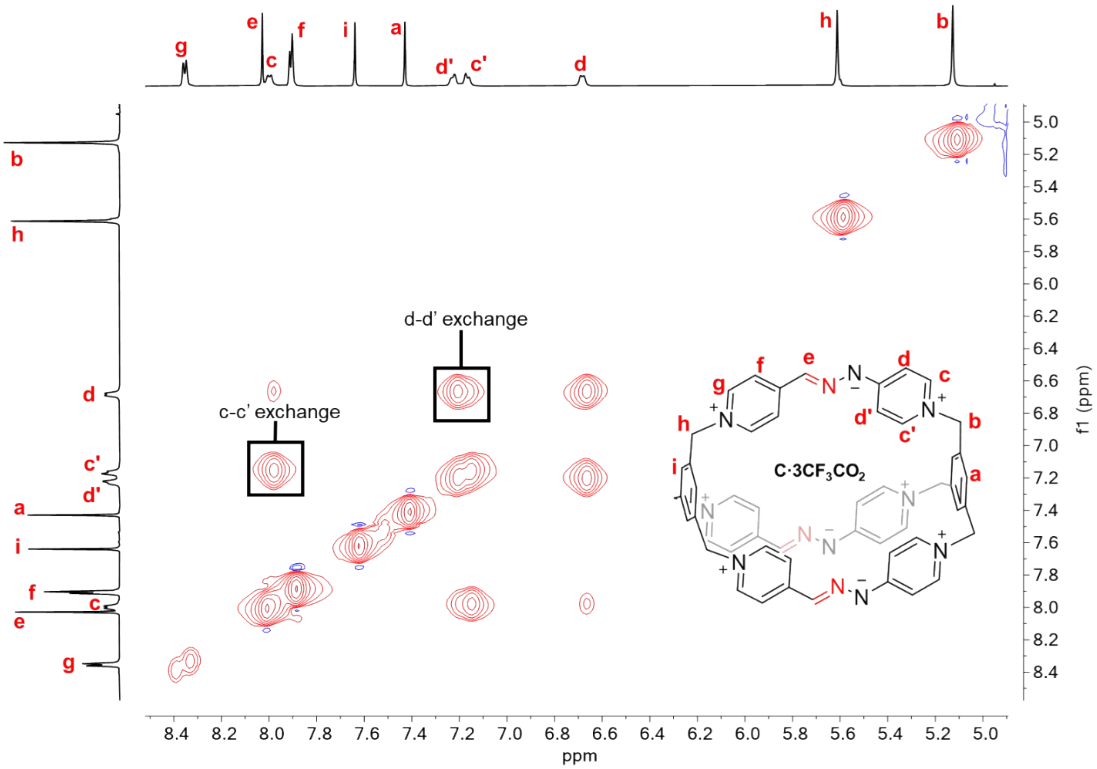

Figure S32. ^{1}H-^{1}H NOESY (500 MHz, D_2O, 298 K) spectrum of **C**·3CF_3CO_2. Exchange cross-peak is labeled in the spectrum.

- **C**·6CF_3CO_2 characterization in CD_3CN with 1 eq of CF_3CO_2D by NMR.

^{1}H NMR (500 MHz, CD_3CN) δ (ppm): 14.94 (s, 3H), 8.61 (d, J = 6.5 Hz, 6H), 8.58 (s, 3H), 8.43 (dd, J = 7.1, 1.8 Hz, 3H), 8.17 (d, J = 6.6 Hz, 6H), 7.82 (s, 3H), 7.72 (dd, J = 7.4, 1.8 Hz, 3H), 7.65 (dd, J = 7.5, 2.6 Hz, 3H), 7.64 (s, 3H), 7.56 (dd, J = 7.1, 2.6 Hz, 3H), 5.68 (s, 6H), 5.38 (s, 6H).

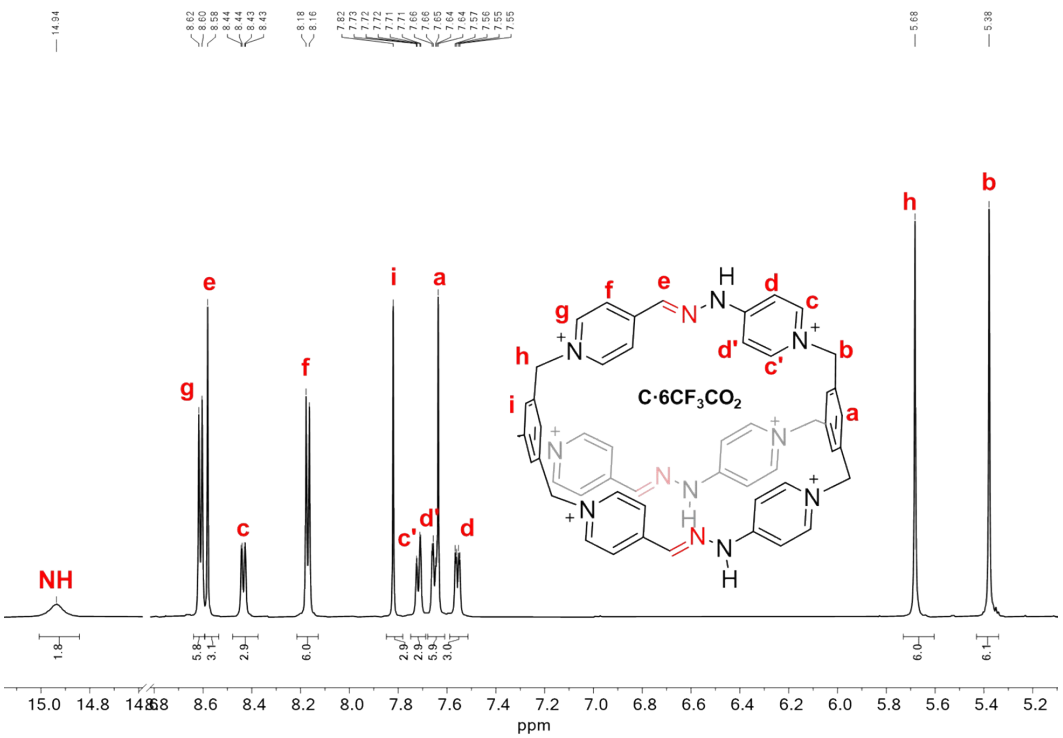

Figure S33. ^{1}H NMR (500 MHz, CD_3CN, 298 K) spectrum of **C**·$6CF_3CO_2$ with 1 eq. of CF_3CO_2D.

- **C**·$3CF_3CO_2$ characterization in CD_3CN with 1 eq of Et_3N by NMR.

^{1}H NMR (400 MHz, CD_3CN) δ (ppm): 8.48 (brs, 3H), 8.42 (d, J = 6.4 Hz, 6H), 8.34 (d, J = 6.6 Hz, 6H), 8.24 (s, 3H), 7.99 (brs, 3H), 7.83 (s, 3H), 7.71 (s, 3H), 7.58 (brs, 3H), 7.30 (brs, 3H), 5.73 (s, 6H), 5.48 (s, 6H).

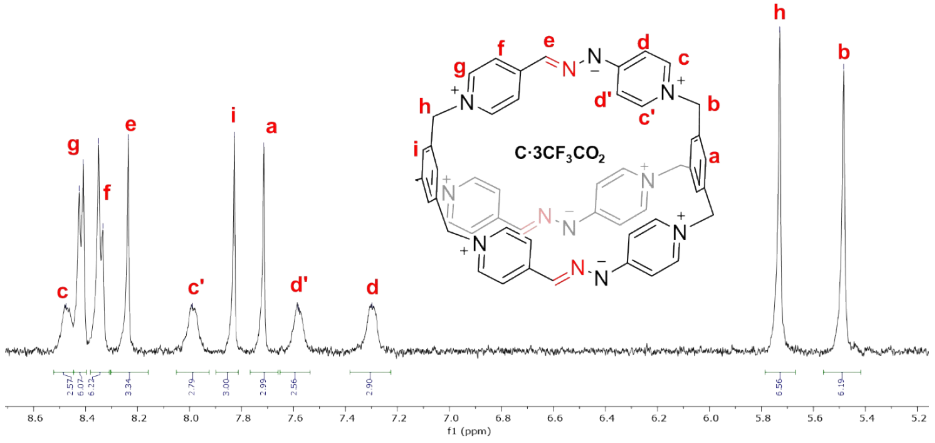

Figure S34. ^{1}H NMR (400 MHz, CD_3CN, 298 K) spectrum of **C**·$3CF_3CO_2$ with 1 eq. of Et_3N.

- **C·6CF$_3$CO$_2$** characterization in MeOD by NMR.

^{1}H NMR (400 MHz, MeOD) δ 8.93 (d, *J* = 6.7 Hz, 6H), 8.80 (dd, *J* = 7.2, 1.7 Hz, 3H), 8.31 (d, *J* = 6.8 Hz, 6H), 8.28 (s, 3H), 8.08 (dd, *J* = 7.3, 1.7 Hz, 3H), 7.98 (s, 3H), 7.82 (s, 3H), 7.72 (dd, *J* = 7.4, 2.8 Hz, 3H), 7.28 (dd, *J* = 7.1, 2.8 Hz, 3H) 5.88 (s, 6H), 5.60 (s, 6H).

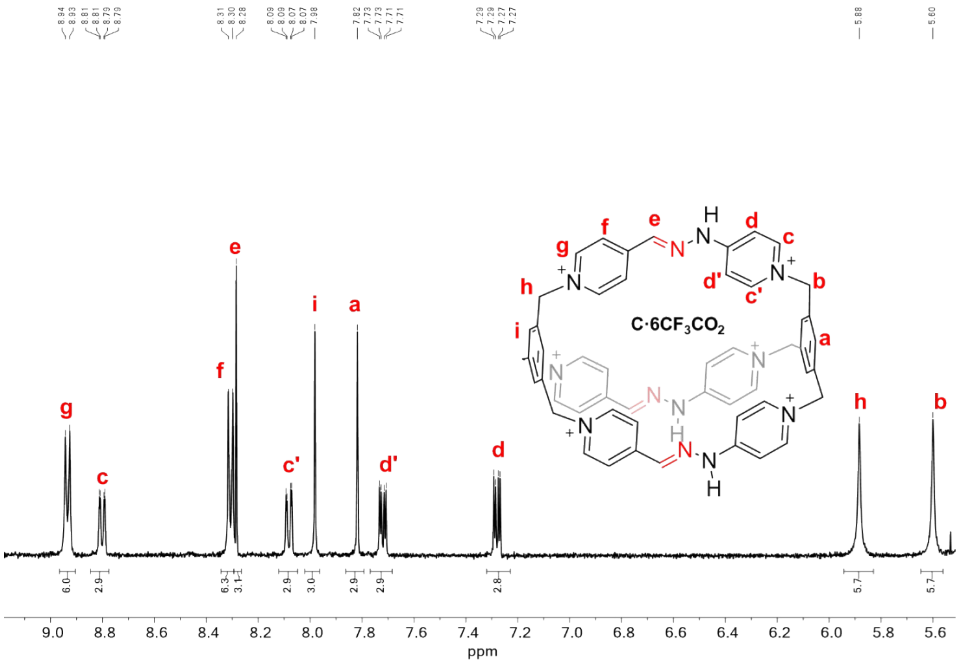

Figure S35. ^{1}H NMR (400 MHz, MeOD, 298 K) spectrum of **C**·6CF$_3$CO$_2$.

3. Acid-base studies of the Red Cage.

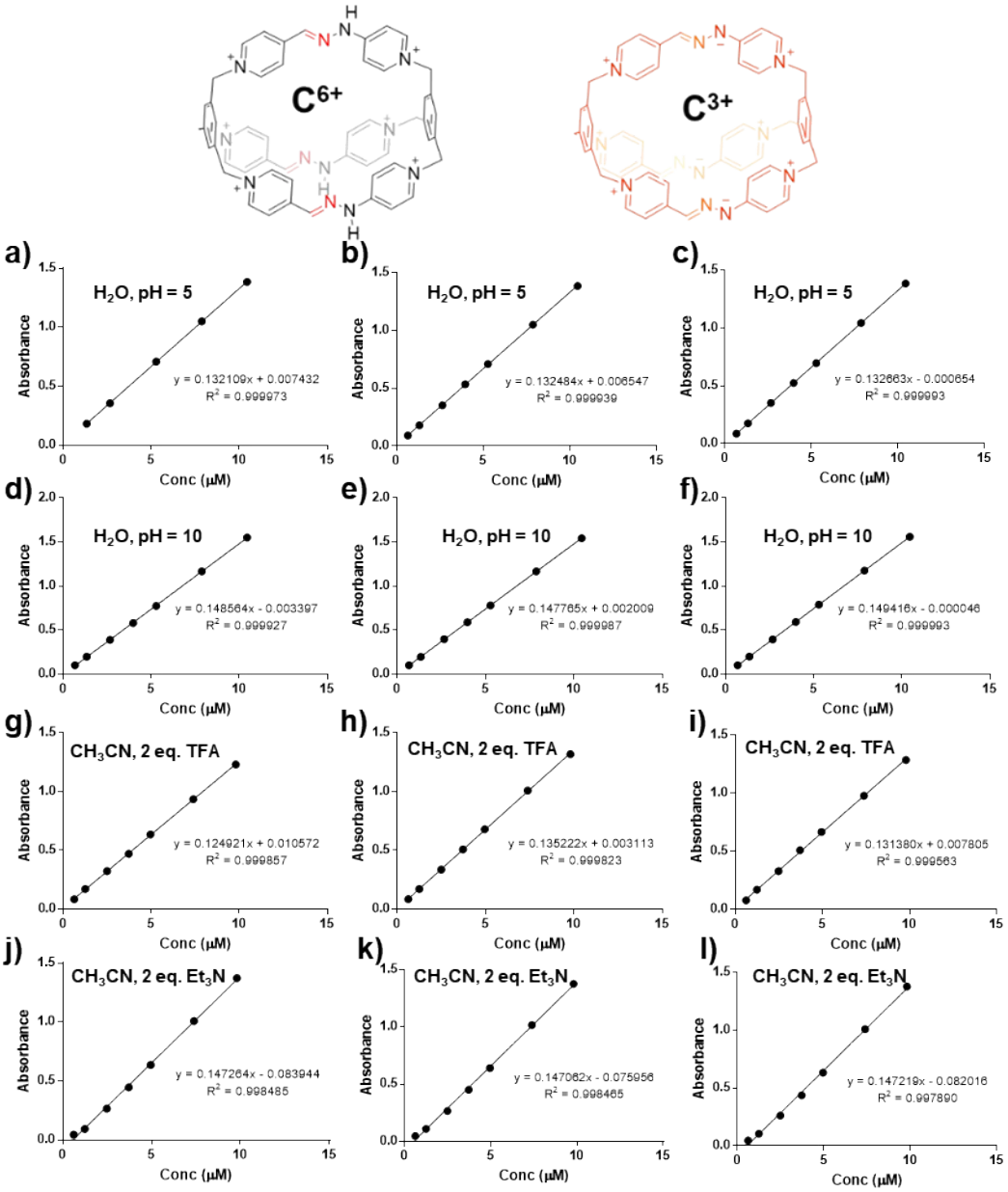

Figure S36. a-c) Linear relationship between absorbance at 358 nm and concentration of **C^{6+}** at pH 5 in H_2O, where $\varepsilon = (132.4 \pm 0.3) \times 10^3$ $Lmol^{-1}com^{-1}$. d-f) Linear relationship between absorbance at 448 nm and concentration of **C^{3+}** at pH 10 in H_2O, where $\varepsilon = (148.6 \pm 0.8) \times 10^3$ $Lmol^{-1}com^{-1}$. g-i) Linear relationship between absorbance at 356 nm and concentration of **C^{6+}** with 2 eq. of TFA in CH_3CN, where $\varepsilon = (130.5 \pm 5.2) \times 10^3$ $Lmol^{-1}com^{-1}$. j-l) Linear relationship between absorbance at 478 nm and concentration of **C^{3+}** with 2 eq. of Et_3N in CH_3CN, where $\varepsilon = (147.2 \pm 0.1) \times 10^3$ $Lmol^{-1}com^{-1}$.

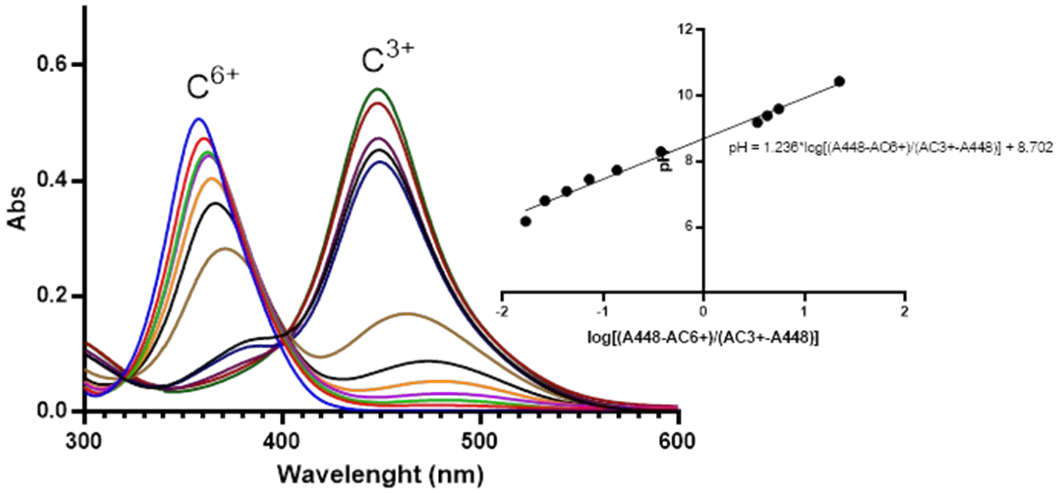

Figure S37. UV-Vis spectra for the titration of **C**·$6CF_3CO_2$ at 4.5 μM in NaH_2PO_4/Na_2HPO_4 and $NaHCO_3/Na_2CO_3$ buffer. **Inset:** Linear fitting of pH plotted against $\log[(A_{448}-A_{C6+})/(A_{C3+}-A_{448})]$, where p$K_a$ value is 8.70.

pH (measured)	V (μL) solution A	V (μL) solution B	V (μL) solution C	V (μL) solution D	Abs (448 nm)	$\log[(A_{448}-A_{C6+})/(A_{C3+}-A_{448})]$
4,79	750	-	-	-	0,0015828	-
6,18	660	90	-	-	0,0108634	-1,770815446
6,81	469	281	-	-	0,0159067	-1,578311243
7,10	375	375	-	-	0,0247537	-1,362288382
7,46	210	540	-	-	0,0393557	-1,138001254
7,74	113	637	-	-	0,0688287	-0,862125922
8,30	45	705	-	-	0,1535647	-0,425457217
9,19	-	-	750	-	0,4316977	0,530893575
9,40	-	750	-	-	0,452876	0,631219915
9,60	-	-	675	75	0,4734347	0,744703678
10,44	-	-	375	375	0,5344227	1,34729122
10,96	-	-	150	600	0,5583727	-

Solution A: 4.5 μM of **C·6CF$_3$CO$_2$** and 0.05 M of NaH_2PO_4. **Solution B**: 4.5 μM of **C·6CF$_3$CO$_2$** and 0.05 M of Na_2HPO_4. **Solution C:** 4.5 μM of **C·6CF$_3$CO$_2$** and 0.05 M of $NaHCO_3$. **Solution D**: 4.5 μM of **C·6CF$_3$CO$_2$** and 0.05 M of Na_2CO_3.

Table S1. Experimental data obtained for the UV-Vis titration of **C**·$6CF_3CO_2$ at 4.5 μM in NaH_2PO_4/Na_2HPO_4 and $NaHCO_3/Na_2CO_3$ buffer.

4. Determination of the energy of the rotational barrier ($\Delta G^{\neq}$).

The coalescence temperature (T_c) could be estimated for different protons on VT NMR experiments. This provides, in association with the maximum peak separation ($\Delta\nu$ in Hz) at slow exchange between **c** – **c'** and **d** – **d'**, the energy of the rotational barrier using Equation (1).[S1]

$$\Delta G^{\neq} = 4.57 \cdot 10^{-3} T_c (9.972 + \log T_c/\Delta\nu) \qquad (1)$$

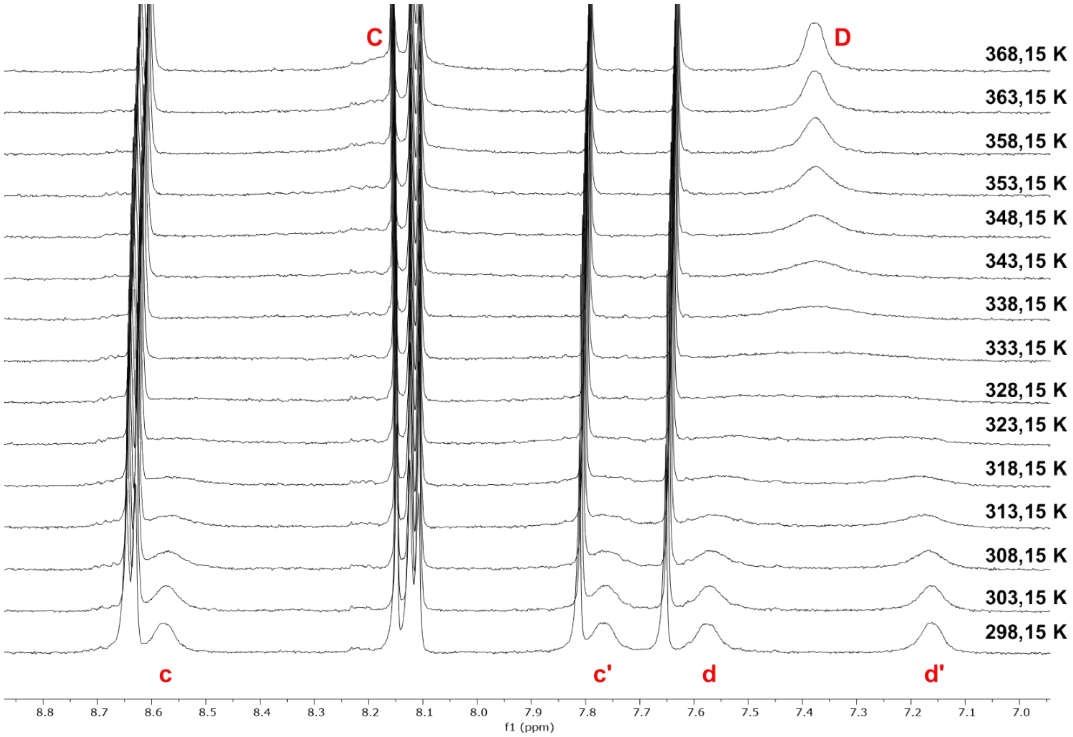

Figure S38. VT ^{1}H NMR (500 MHz, D_2O, 298 K) stacked spectra for **C**·$6CF_3CO_2$.

Signal	$\Delta\nu_c$ (Hz)	T_c (K)	$\Delta G^{\neq}$ (kcal mol^{-1})
c – c'	326,14	343,15	15,7
d – d'	164,45	333,15	15,5

Table S2. Experimental data obtained for the calculation of $\Delta G^{\neq}$ via coalescence temperatures of various signals on the VT ^{1}H NMR of **C**·$6CF_3CO_2$ in water.

5. Guest recognition ability of C·6Cl.

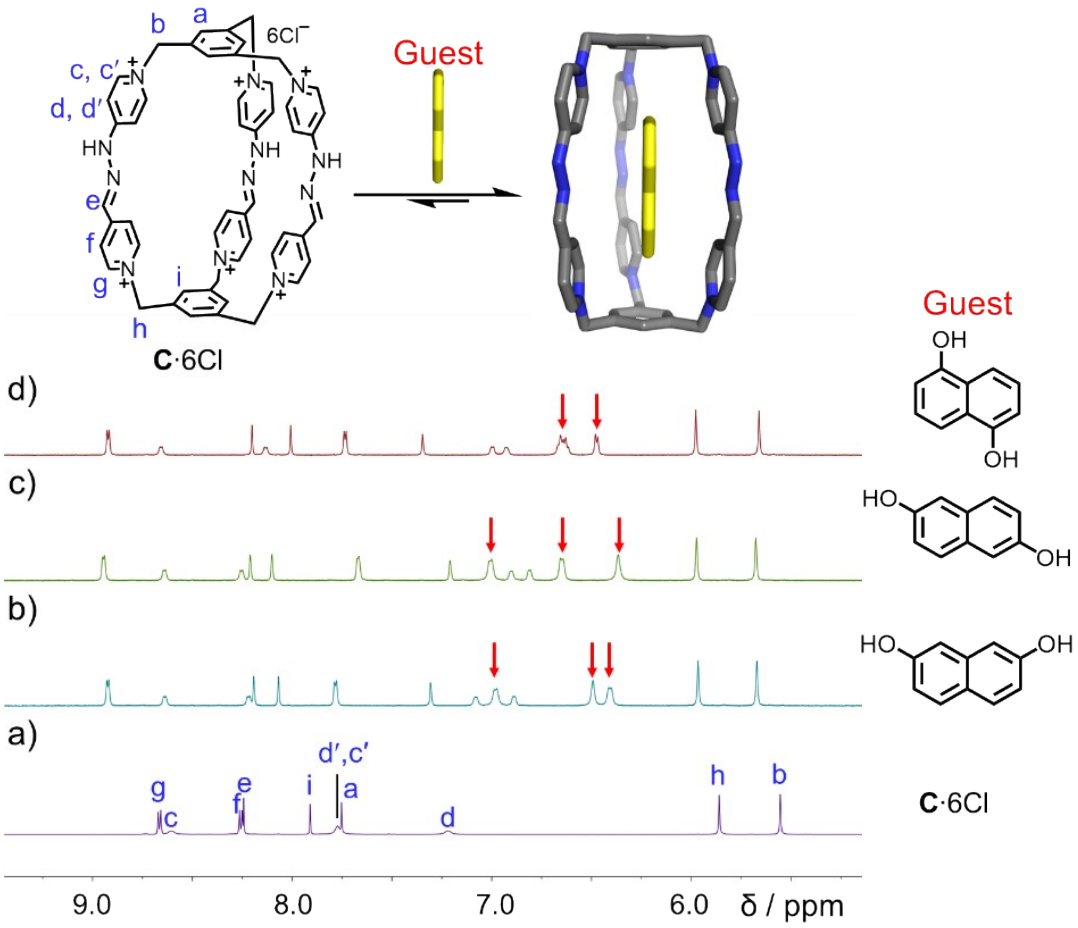

Figure S39. ^{1}H NMR spectrum (500 MHz, D_2O, 298 K) of a) **C**·6Cl, b) **C**·6Cl with **2,7-DHN** (2 eq), c) **C**·6Cl with **2,6-DHN** (2 eq) and d) **C**·6Cl with **1,5-DHN** (2 eq.).

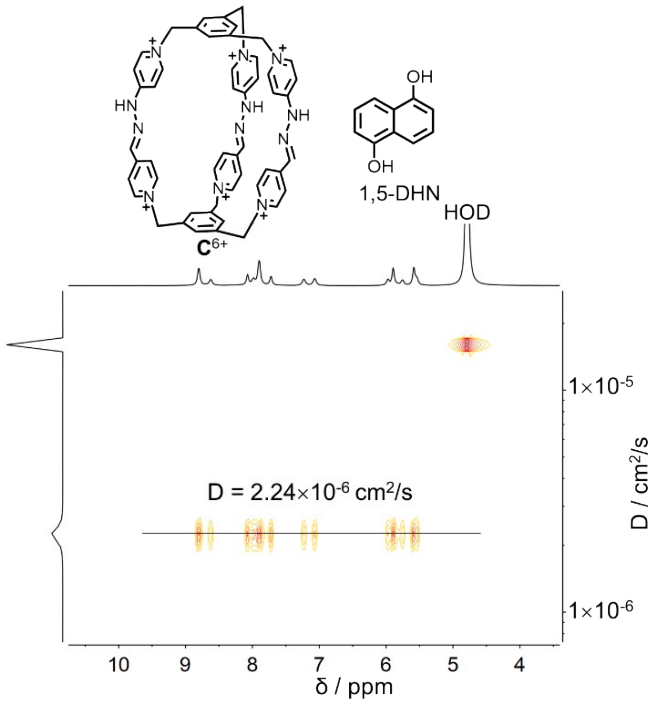

Figure S40. ^{1}H DOSY spectrum of 1:1 mixture of **1,5-DHN** and **C**·6Cl. The spectrum demonstrates that both **1,5-DHN** and **C**·6Cl have the same diffusion coefficient, implying the formation of complex **1,5-DHN** ⊂ **C**·6Cl.

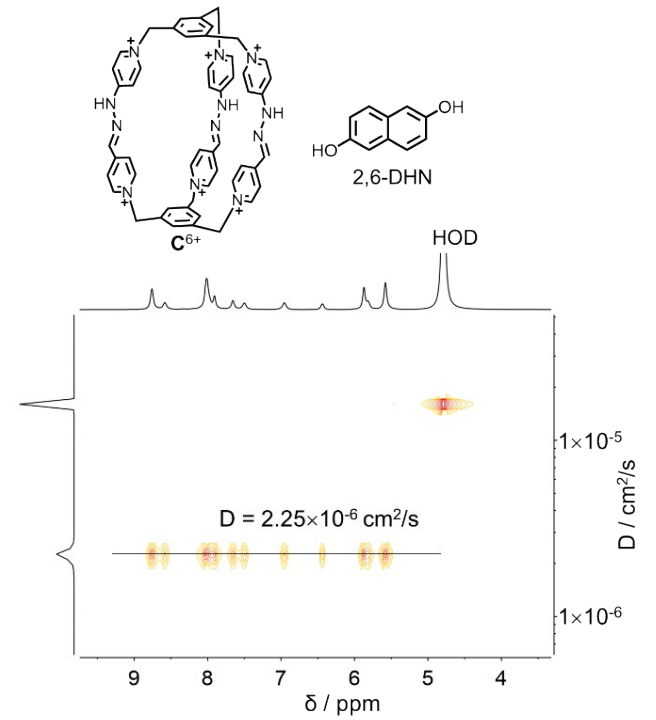

Figure S41. ^{1}H DOSY spectrum of 1:1 mixture of **2,6-DHN** and **C**·6Cl. The spectrum demonstrates that both **2,6-DHN** and **C**·6Cl have the same diffusion coefficient, implying the formation of complex **2,6-DHN** ⊂ **C**·6Cl.

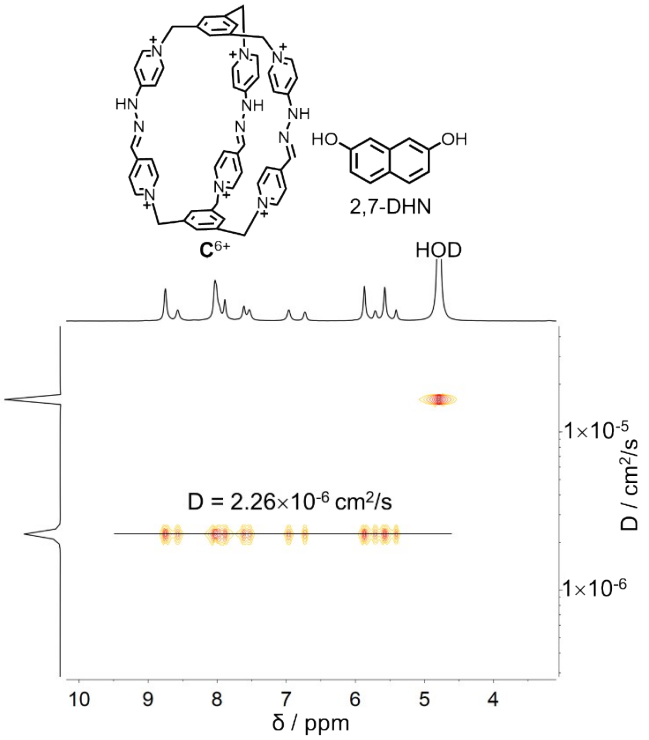

Figure S42. ^{1}H DOSY spectrum of 1:1 mixture of **2,7-DHN** and **C**·6Cl. The spectrum demonstrates that both **2,7-DHN** and **C**·6Cl have the same diffusion coefficient, implying the formation of complex **2,7-DHN** ⊂ **C**·6Cl.

6. ^{1}H NMR titration experiments determination of *K*a value for inclusion complexes in water.

- **1,5-DHN ⊂ C·6Cl.**

^{1}H NMR spectroscopic studies were performed (Figure S43) to calculate the binding constant of **1,5-DHN ⊂ C**·6Cl. We titrated the sample of $\mathbf{C^{6+}}$ with **1,5-DHN** in D_2O. The corresponding ^{1}H NMR spectra demonstrated (Figure S44) that the binding constant is around 1.5 (± 0.2) × 10^4 M^{-1}.

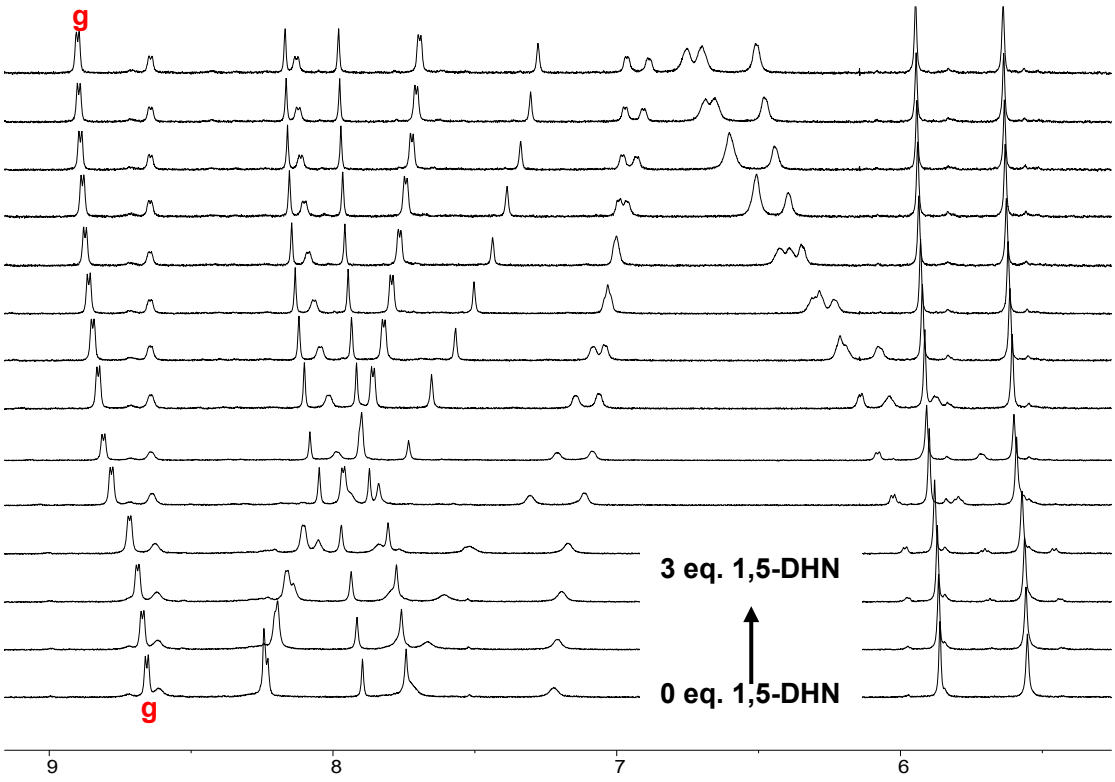

Figure S43. Partial ^{1}H NMR spectra (600 MHz, D_2O, 298 K) of **C**·6Cl upon addition of 0-3 eq. of **1,5-DHN**. [**C**·6Cl] = 0.5 mM for all spectra.

The mechanism proposed for the fitting process equilibria, and introduced on the software *Dynafit* was the following:[S2] $\mathbf{C^{6+}}$ **+ 2.7-DHN <=> 2.7-DHN⊂$\mathbf{C^{6+}}$**

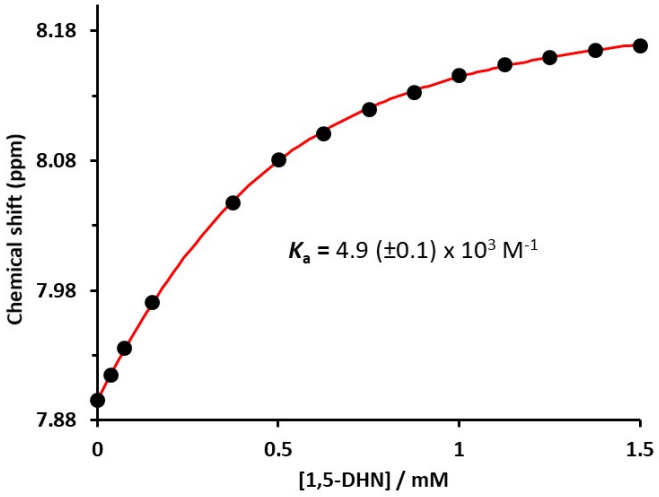

Figure S44. Fitting of the experimental data (circles) of signal H_g.

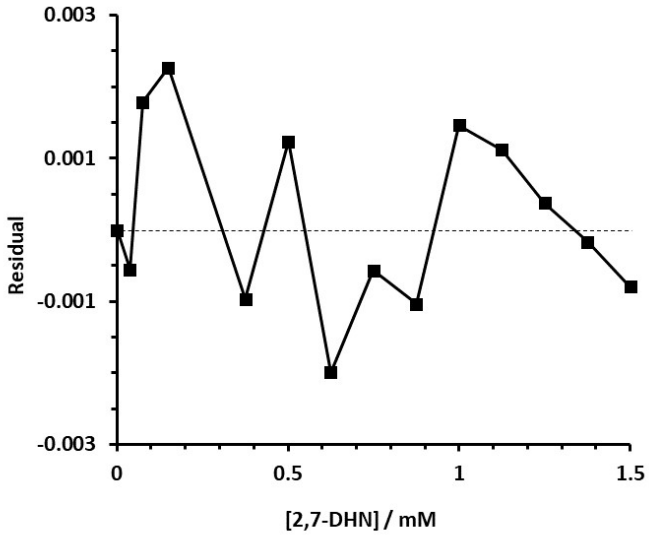

Figure S45. Residuals of the fitting of signal H_g.

- **2,6-DHN ⊂ C·6Cl.**

^{1}H NMR spectroscopic studies were performed (Figure S45) to calculate the binding constant of **2,6-DHN ⊂ C·6Cl**. We titrated the sample of $\mathbf{C^{6+}}$ with **2,6-DHN** in D_2O. The corresponding ^{1}H NMR spectra demonstrated (Figure S46) that the binding constant of **2,6-DHN ⊂ C·6Cl** is around 4.0 (± 0.2) × 10^3 M^{-1}.

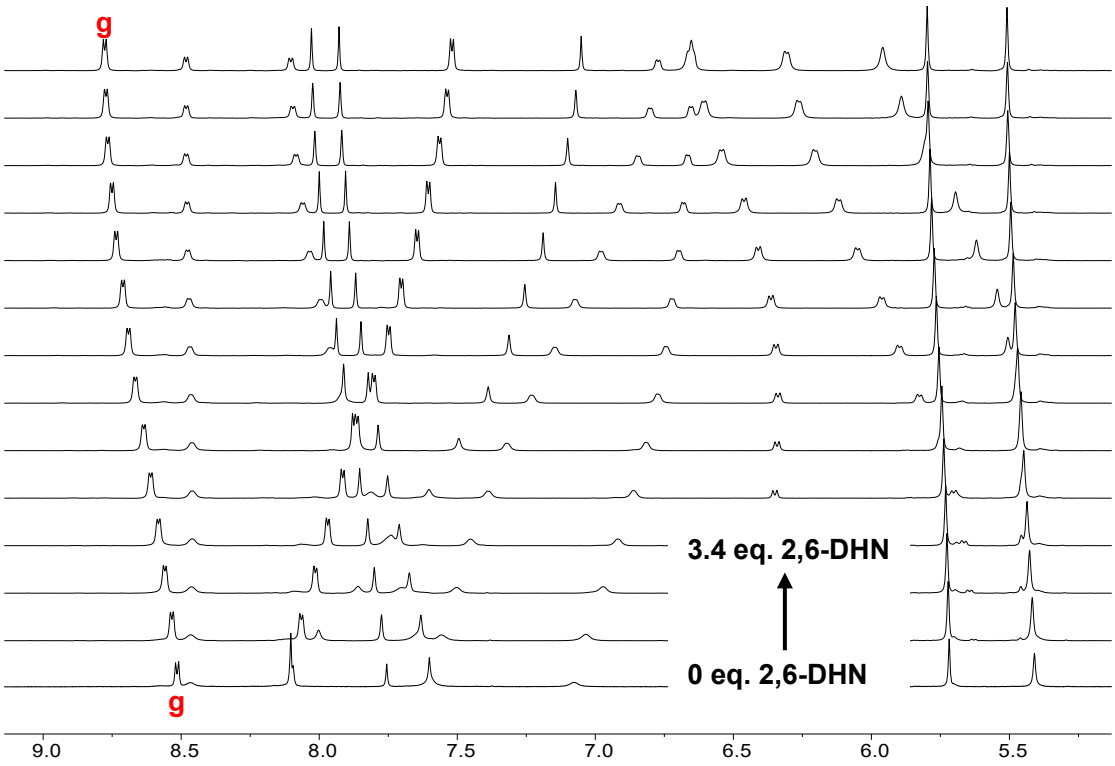

Figure S46. Partial ^{1}H NMR spectra (600 MHz, D_2O, 298 K) of **C**·6Cl upon addition of 0-3.4 eq. of **2,6-DHN**. [**C**·6Cl] = 0.5 mM for all spectra.

The mechanism proposed for the fitting process equilibria, and introduced on the software *Dynafit* was the following:[S2] $\mathbf{C^{6+}}$ **+ 2.6-DHN <=> 2.6-DHN⊂**$\mathbf{C^{6+}}$

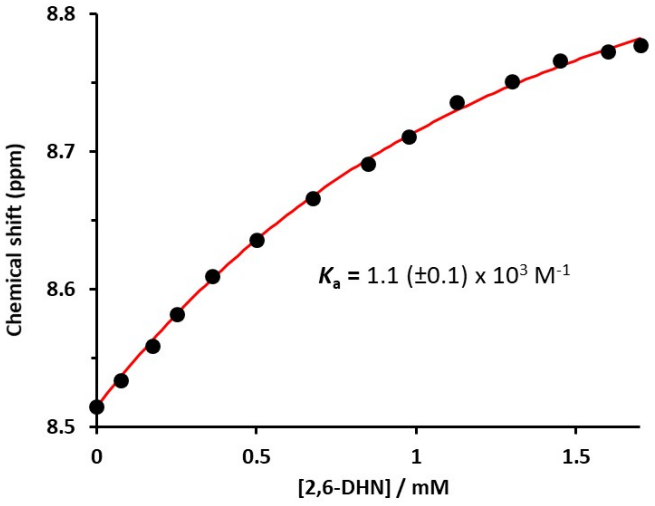

Figure S47. Fitting of the experimental data (circles) of signal H_g.

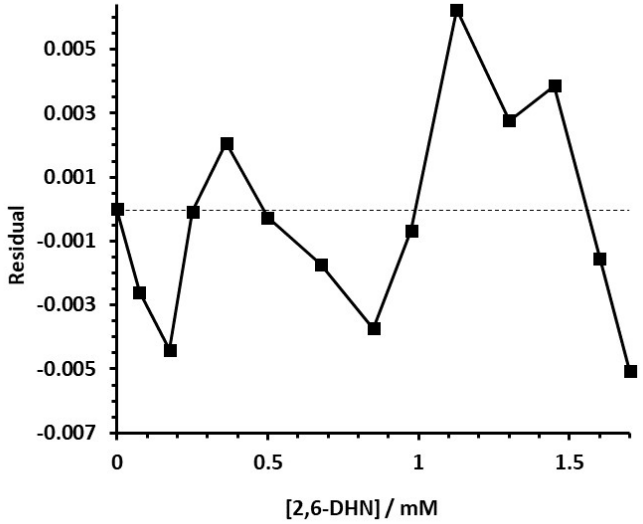

Figure S48. Residuals of the fitting of signal H_g.

- **2,7-DHN ⊂ C·6Cl.**

^{1}H NMR spectroscopic studies were performed (Figure S47) to calculate the binding constant of **2,7-DHN ⊂ C**·6Cl. We titrated the sample of $\mathbf{C^{6+}}$ with **2,7-DHN** in D_2O. The corresponding ^{1}H NMR spectra demonstrated (Figure S48) that the binding constant of **2,7-DHN ⊂ C**·6Cl is around 1.2 (± 0.3) × 10^4 M^{-1}.

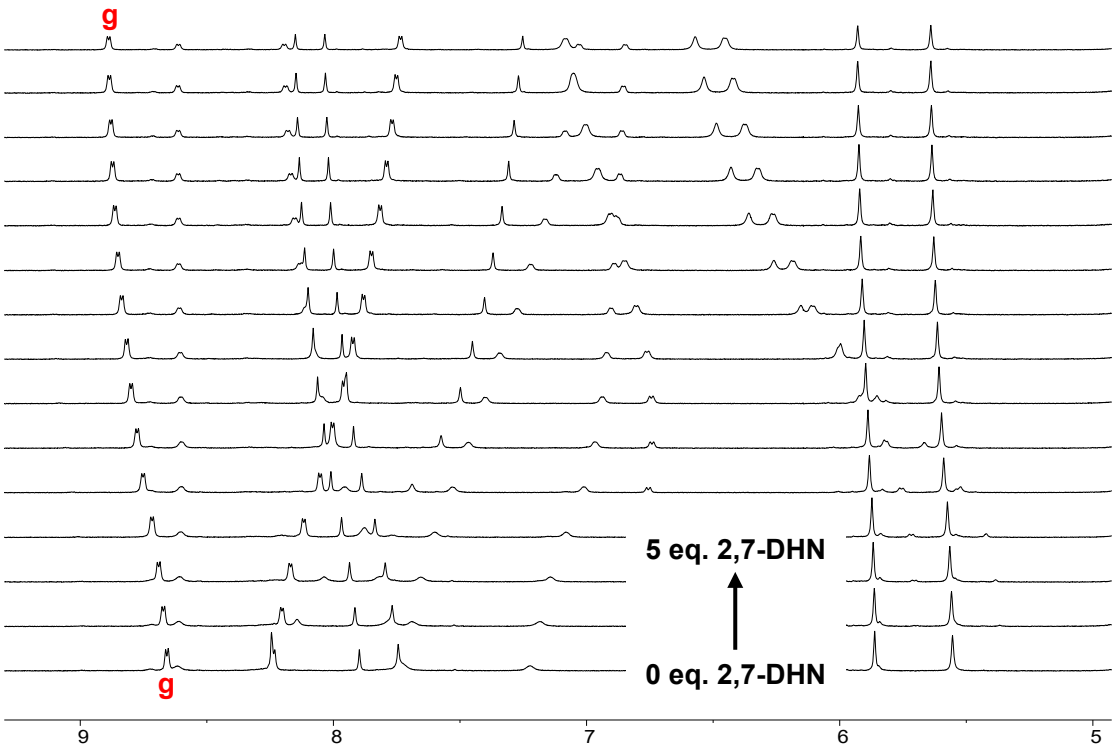

Figure S49. Partial ^{1}H NMR spectra (600 MHz, D_2O, 298 K) of **C**·6Cl upon addition of 0-5 eq. of **2,7-DHN**. [**C**·6Cl] = 0.5 mM for all spectra.

The mechanism proposed for the fitting process equilibria, and introduced on the software *Dynafit* was the following:[S2] $\mathbf{C^{6+}}$ **+ 2.7-DHN <=> 2.7-DHN⊂**$\mathbf{C^{6+}}$

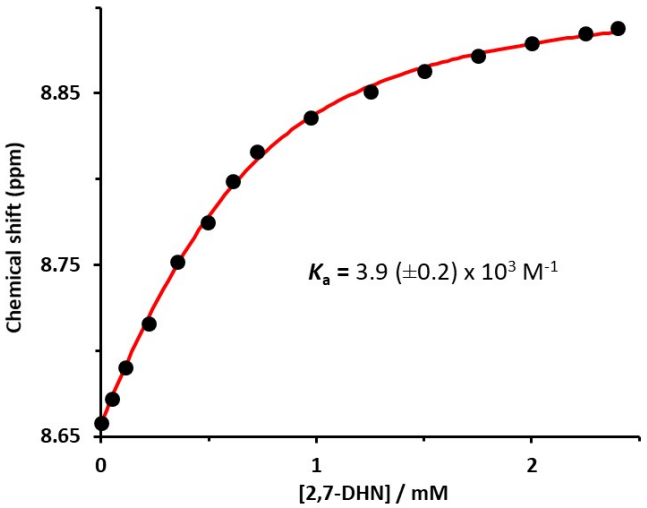

Figure S50. Fitting of the experimental data (circles) of signal H_g.

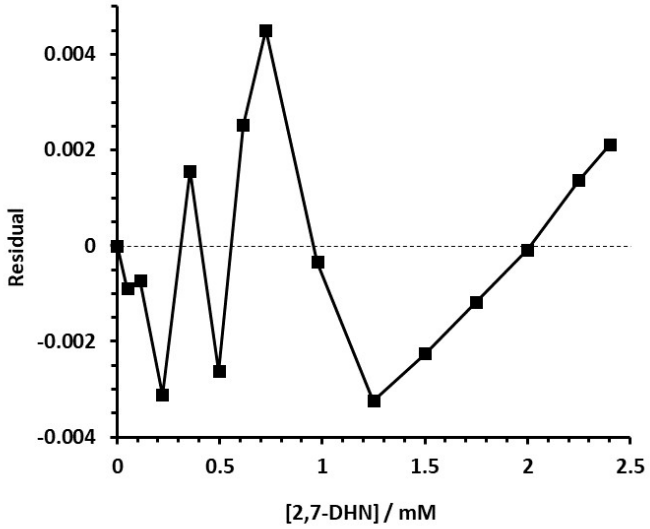

Figure S51. Fitting of the experimental data (circles) of signal H_g.

- **1,5-DHNc ⊂ C·6CF_3CO_2 at pD = 2.**

To carry out the titration, mixture of **C**·6CF_3CO_2 and 1,5-DHNc of different proportion were prepared from appropriate stocks solutions in NaH_2PO_4/H_3PO_4 buffer at pD = 2.

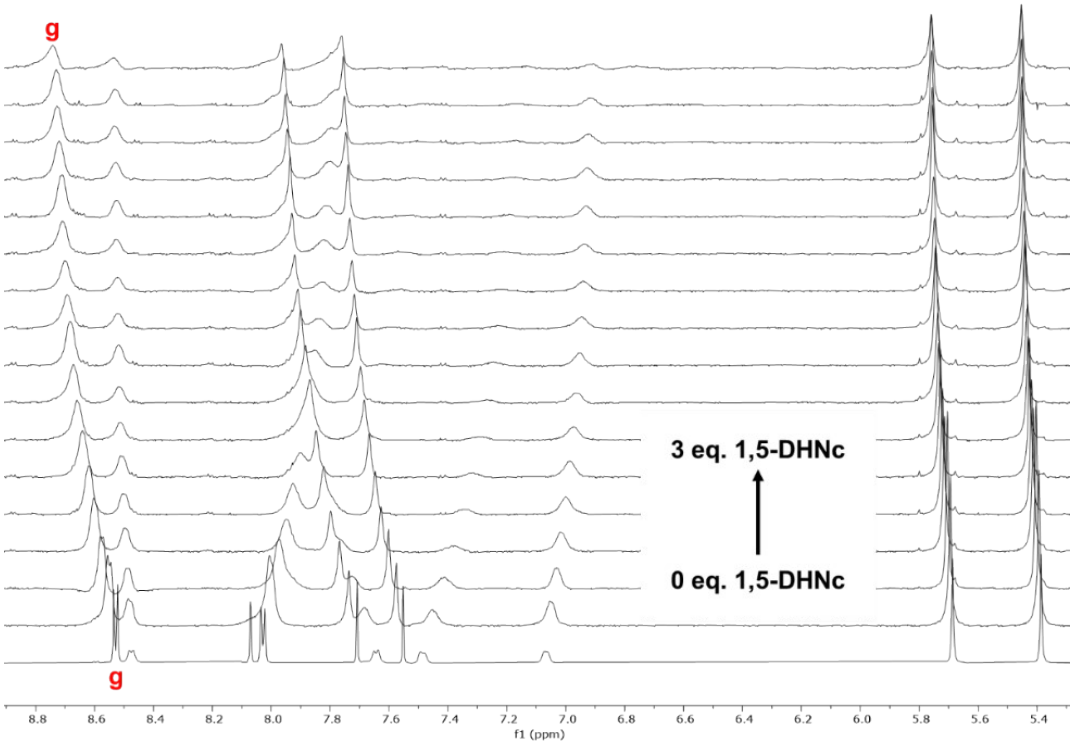

Figure S52. ^{1}H NMR (500 MHz, D_2O, 298 K) spectra of **C**·6CF_3CO_2 (0.5 mM) upon titration with 1,5-DHNc.

The mechanism proposed for the fitting process equilibria and introduced on the software *Dynafit* was the following:[S2] **C^{6+} + 1.5-DHNc <=> 1.5-DHNc⊂C^{6+}**

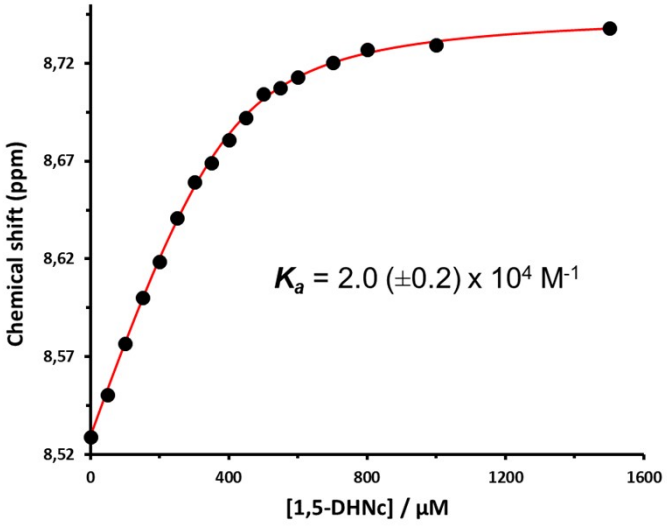

Figure S53. Fitting of the experimental data (circles) of signal H_g.

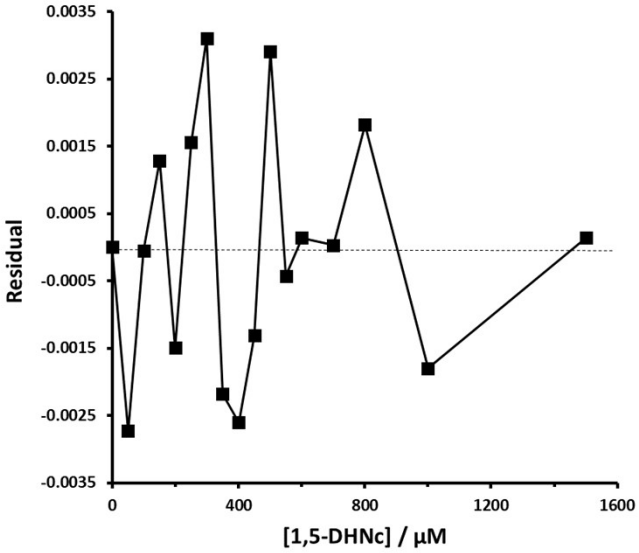

Figure S54. Residuals of the fitting of signal H_g.

- **1,5-DHNc ⊂ C·6CF_3CO_2 at pD = 12.**

To carry out the titration, mixture of **C**·3CF_3CO_2 and 1,5-DHNc of different proportion were prepared from appropriate stocks solutions in Na_3PO_4/Na_2HPO_4 buffer at pD = 12.

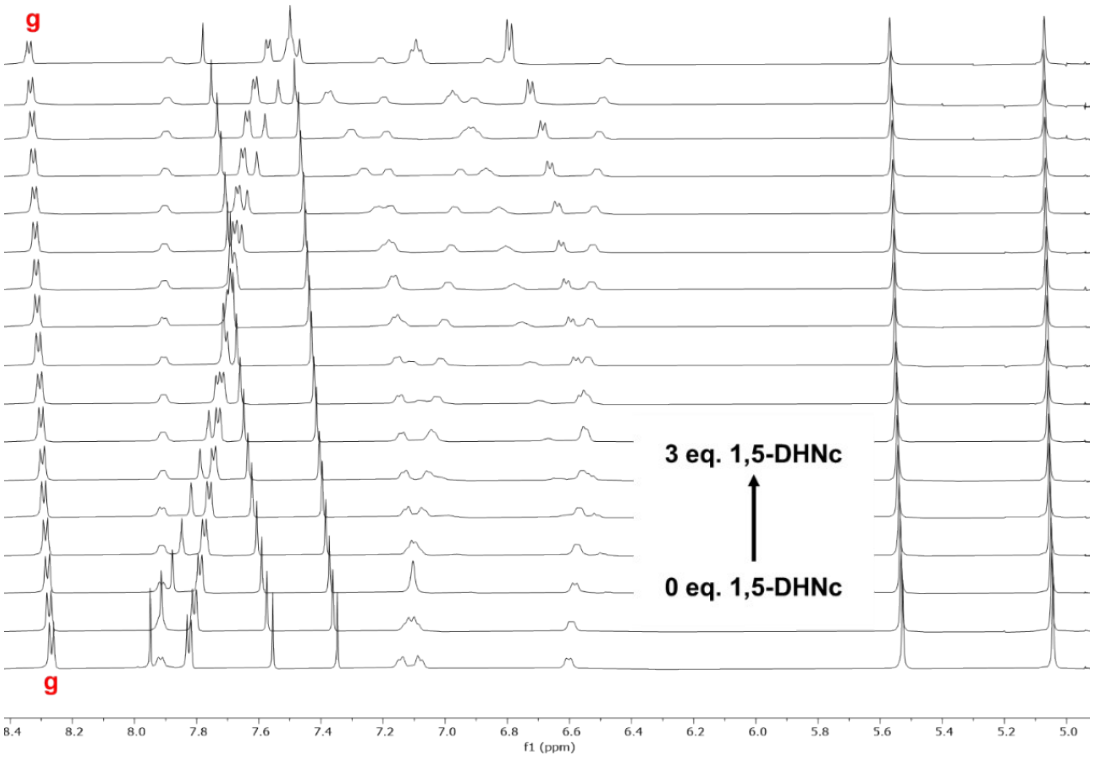

Figure S55. ^{1}H NMR (500 MHz, D_2O, 298 K) spectra of **C**·3CF_3CO_2 (0.5 mM) upon titration with 1,5-DHNc.

The mechanism proposed for the fitting process equilibria, and introduced on the software *Dynafit* was the following:[S2] **C^{3+} + 1.5-DHNc <=> 1.5-DHNc⊂C^{3+}**

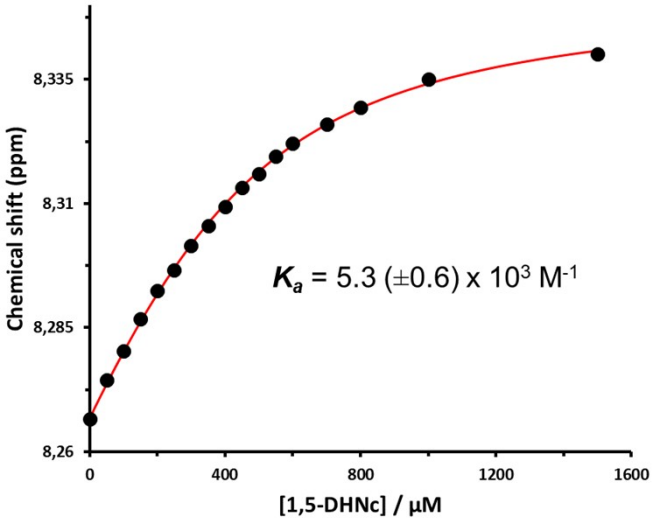

Figure S56. Fitting of the experimental data (circles) of signal H_g.

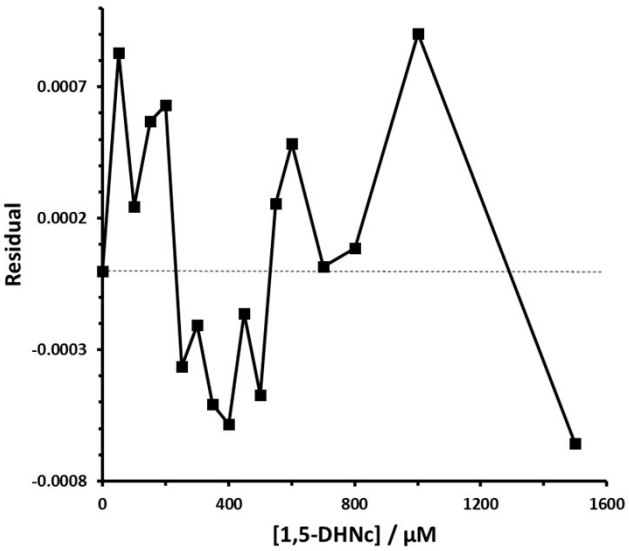

Figure S57. Residuals of the fitting of signal H_g.

7. X-ray Crystallography

1) **C**·6Cl

a) Methods

Single crystals of **C**·6Cl, suitable for X-ray crystallography, were grown by slow vapor diffusion of acetone into solution of $\mathbf{C}^{6+}$ (in water) over the course of days. Data were collected at 170 K on a Bruker APEX-II CCD Diffractometer equipped with a GaKα IμS source and MX optic.

b) Crystal parameters

$[C_{51}H_{56}Cl_6N_{12}O_4]$, red block (0.16×0.08×0.06mm), Triclinic, space group P-1, a = 10.6132(19) Å, b = 15.730(3) Å, c = 21.174(4) Å, α = 83.737(6)°, β = 78.244(7)°, γ = 89.362(5)°, V = 3440.0(11) Å^3, Z = 2, T = 170 K, ρ_{calc} = 1.075 g/cm^3, μ(GaKα) = 1.34139 mm^{-1}. A total of 29893 reflections were collected, of which 11269 were unique. Final $R_1(wR_2)$ [$I > 2\sigma(I)$] = 0.1421(0.3164) and $R_1(wR_2)$ (all data) = 0.2506(0.3924). The structure was solved by direct method and different Fourier syntheses. Using Olex2[S3], the structure was solved with the ShelXT[S4] structure solution program using Intrinsic Phasing and refined with the ShelXL[S5] refinement package using Least Squares minimization. CCDC number: 1988842.

c) Solid-state structure

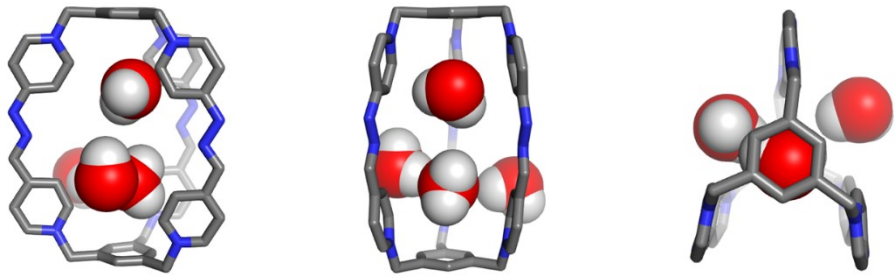

Figure S58. Different views of the solid-state structure of **C**·6Cl. Carbon, grey; nitrogen blue; red, oxygen; Hydrogen, white. Hydrogen atoms of para-capsule $\mathbf{C}^{6+}$, other counterions and disordered solvent molecules are omitted for clarity.

2) **2,7-DHN** ⊂ $\mathbf{C}^{6+}$

a) Methods

Single crystals of **2,7-DHN** ⊂ $\mathbf{C}^{6+}$, suitable for X-ray crystallography, were grown by slow

vapor diffusion of acetone into solution of **2,7-DHN ⊂ C^{6+}** (in water) over the course of days. Data were collected at 170 K on a Bruker APEX-II CCD Diffractometer equipped with a GaKα IμS source and MX optic.

b) Crystal parameters

$[C_{61}H_{54}Cl_4N_{12}O_2]$, red block (0.08 × 0.06 × 0.05mm), Triclinic, space group P-1, a = 10.4351(5) Å, b = 15.6984(7) Å, c = 20.2493(8) Å, α = 78.582(3)°, β = 79.242(3)°, γ = 88.796(3)°, V = 3193.9(2) Å^3, Z = 2, T = 170 K, ρ_{calc} = 1.174 g/cm^3, μ(GaKα) = 1.34139 mm^{-1}. A total of 33571 reflections were collected, of which 11962 were unique. Final $R_1(wR_2)$ [$I > 2\sigma(I)$] = 0.1619(0.3347) and $R_1(wR_2)$ (all data) = 0.3238(0.4302). T The structure was solved by direct method and different Fourier syntheses. Using Olex2, [S3] the structure was solved with the ShelXT[S4] structure solution program using Intrinsic Phasing and refined with the ShelXL[S5] refinement package using Least Squares minimization. CCDC number: 1988362.

c) Solid-state structure

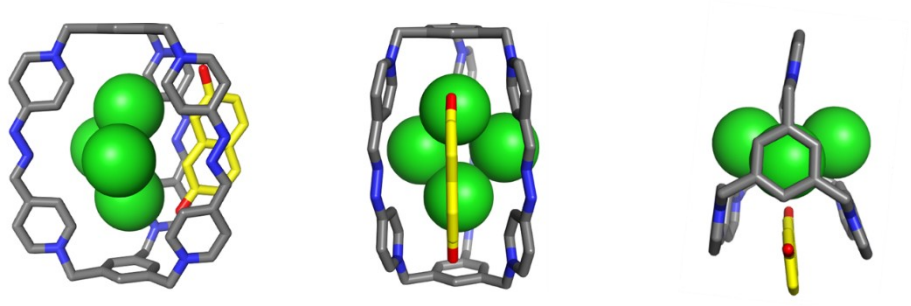

Figure S59. Different views of the solid-state structure of **2,7-DHN ⊂ C^{6+}.** Carbon, grey in the host and yellow in the guest; nitrogen, blue; red, oxygen. Hydrogen atoms and disordered solvent molecules are omitted for clarity.

8. References

S1. a) J. Sandstrom, *Dynamic NMR Spectroscopy*; Academic Press: New York, NY, USA, **1983**. b) H. Kessler, *Angew. Chem. Int. Ed.* **1970**, *9*, 219-235.

S2. P. Kuzmic, *Anal.* Biochem **1996**, *237,* 260-273

S3. Dolomanov, O. V.; Bourhis, L. J.; Gildea, R. J.; Howard, J. A. K.; Puschmann, H. *J. Appl. Cryst.* **2009**, *42*, 339-341.

S4. Sheldrick, G. M. *Acta Cryst.* **2015**, *A71*, 3-8.

S5. Sheldrick, G. M. *Acta Cryst.* **2015**, *C71*, 3-8.